Jahn–Teller effect in van der Waals complexes; Ar–C6H6+ and Ar–C6D6+

Ad van der Avoird and Victor F. Lotrich

Citation: J. Chem. Phys. **120**, 10069 (2004); doi: 10.1063/1.1714793
View online: http://dx.doi.org/10.1063/1.1714793
View Table of Contents: http://jcp.aip.org/resource/1/JCPSA6/v120/i21
Published by the American Institute of Physics.

Additional information on J. Chem. Phys.

Journal Homepage: http://jcp.aip.org/
Journal Information: http://jcp.aip.org/about/about_the_journal
Top downloads: http://jcp.aip.org/features/most_downloaded
Information for Authors: http://jcp.aip.org/authors

ADVERTISEMENT

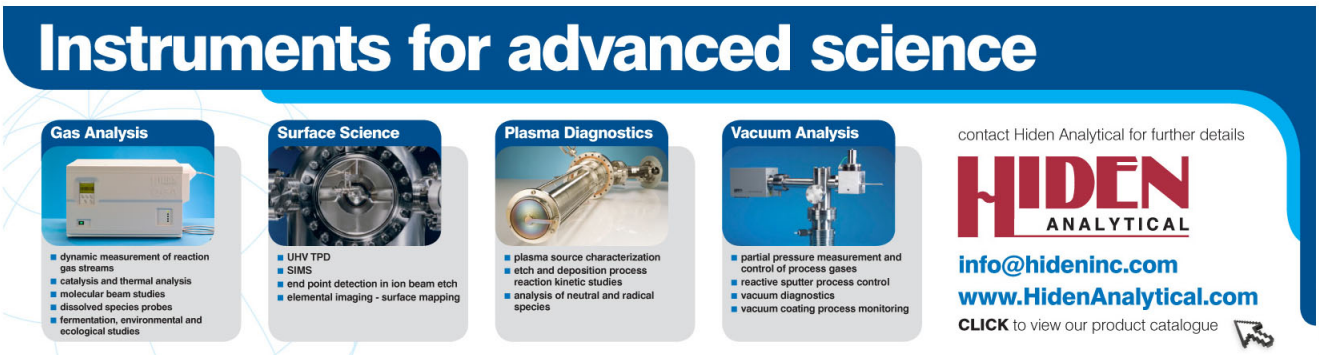

Downloaded 11 Feb 2013 to 131.174.248.95. Redistribution subject to AIP license or copyright; see http://jcp.aip.org/about/rights_and_permissions

HTML ABSTRACT + LINKS

Jahn–Teller effect in van der Waals complexes: Ar–$C_6H_6^+$ and Ar–$C_6D_6^+$

Ad van der Avoird[a] and Victor F. Lotrich[b]
Institute of Theoretical Chemistry, NSRIM, University of Nijmegen, Toernooiveld, 6525 ED Nijmegen, The Netherlands

(Received 15 January 2004; accepted 3 March 2004)

The two asymptotically degenerate potential energy surfaces of argon interacting with the $\tilde{X}\,^2E_{1g}$ ground state benzene$^+$ cation were calculated *ab initio* from the interaction energy of the neutral Ar–benzene complex given by Koch *et al.* [J. Chem. Phys. **111**, 198 (1999)] and the difference of the geometry-dependent ionization energies of the complex and the benzene monomer computed by the outer valence Green's function method. Coinciding minima in the two potential surfaces of the ionic complex occur for Ar on the C_{6v} symmetry axis of benzene$^+$ (the z axis) at $z_e=3.506$ Å. The binding energy D_e of 520 cm^{-1} is only 34% larger than the value for the neutral Ar–benzene complex. The higher one of the two surfaces is similar in shape to the neutral Ar–benzene potential, the lower potential is much flatter in the (x,y) bend direction. Nonadiabatic (Jahn–Teller) coupling was taken into account by transformation of the two adiabatic potentials to a two-by-two matrix of diabatic potentials. This transformation is based on the assumption that the adiabatic states of the Ar–benzene$^+$ complex geometrically follow the Ar atom. *Ab initio* calculations of the nonadiabatic coupling matrix element between the adiabatic states with the two-state-averaged CAS-SCF(5,6) method confirmed the validity of this assumption. The bound vibronic states of both Ar–$C_6H_6^+$ and Ar–$C_6D_6^+$ were computed with this two-state diabatic model in a basis of three-dimensional harmonic oscillator functions for the van der Waals modes. The binding energy $D_0=480$ cm^{-1} of the perdeuterated complex agrees well with the experimental upper bound of 485 cm^{-1}. The ground and excited vibronic levels and wave functions were used, with a simple model dipole function, to generate a theoretical far-infrared spectrum. Strong absorption lines were found at 10.1 cm^{-1} (bend) and 47.9 cm^{-1} (stretch) that agree well with measurements. The unusually low bend frequency is related to the flatness of the lower adiabatic potential in the (x,y) direction. The van der Waals bend mode of e_1 symmetry is quadratically Jahn–Teller active and shows a large splitting, with vibronic levels of A_1, E_2, and A_2 symmetry at 1.3, 10.1, and 50.2 cm^{-1}. The level at 1.3 cm^{-1} leads to a strong absorption line as well, which could not be measured because it is too close to the monomer line. The level at 50.2 cm^{-1} gives rise to weaker absorption. Several other weak lines in the frequency range of 10 to 60 cm^{-1} were found. © *2004 American Institute of Physics.*
[DOI: 10.1063/1.1714793]

I. INTRODUCTION

The argon–benzene complex is a prototype van der Waals complex bound by dispersion forces. A series of experimental and theoretical studies has been devoted to this complex, both in the electronic ground state and in the lowest excited singlet and triplet states.[1–8] Highly accurate three-dimensional intermolecular potential surfaces for all of these states were obtained from *ab initio* calculations[6–8] by the coupled cluster method with singly and doubly excited states and the noniterative inclusion of triples [CCSD(T)]. The frequencies of the van der Waals modes of the complex were computed on these potentials and their comparison with spectroscopic data[2–5] has shown that the *ab initio* potentials are accurate indeed.

The complex of argon with ionized benzene is expected to be drastically different from the neutral species. Binding in cationic complexes is typically an order of magnitude stronger than in the corresponding neutral systems.[9,10] Experiments revealed, however, that the binding of the ionic complex in this case is not much stronger. The binding energies D_e and D_0 are 387 and 328 cm^{-1} in neutral argon–benzene according to the *ab initio* calculations[6] and slightly less according to experiment,[11] while it is known from ionization energies[12] that D_0 is only 170 cm^{-1} larger in the ionic complex. We will show further on in this paper that in both the ionic and neutral systems the equilibrium position of the Ar atom is located on the sixfold symmetry axis of benzene and that the equilibrium distance R_e is only slightly smaller in the ionic complex. Still, there is an important difference with the neutral species caused by the fact that the electronic ground state of the benzene$^+$ cation is twofold degenerate at the D_{6h} symmetric geometry. This cation is a well-known[13–17] and well-studied $E\otimes e$ Jahn–Teller system. The most advanced experimental and theoretical study of the Jahn–Teller effect in both isotopomers $C_6H_6^+$ and $C_6D_6^+$ is by Applegate and Miller.[17] Their paper also summarizes the previous work. The benzene$^+$ cation undergoes distortion of

[a]Electronic mail: avda@theochem.kun.nl
[b]Present address: Quantum Theory Project, University of Florida, P.O. Box 118435, Gainesville, Florida 32611-8435.

 © 2004 American Institute of Physics

Downloaded 11 Feb 2013 to 131.174.248.95. Redistribution subject to AIP license or copyright; see http://jcp.aip.org/about/rights_and_permissions

the D_{6h} symmetry by linear Jahn–Teller coupling with three of the four normal modes of e_{2g} symmetry and quadratic coupling with the modes of e_{1g}, e_{1u}, e_{2g}, and e_{2u} symmetry. This distortion causes a static energy lowering of 717 cm^{-1}, but the threefold barrier in the moat around the D_{6h} structure that would lead to symmetry breaking of the vibrationally averaged structure is very low. Barriers on the order of 10 cm^{-1}, at most, occur for the individual modes,[15,17] and the positive and negative contributions of different modes nearly cancel each other.[17] The vibrational zero-point levels in the Jahn–Teller active modes that would break the symmetry are several hundreds of cm^{-1} above these barriers and the vibronic ground state of benzene$^+$ has nearly perfect D_{6h} symmetry. This is confirmed by a recent rotationally resolved ZEKE photoelectron study[18] that finds perfect D_{6h} symmetry of both $C_6H_6^+$ and $C_6D_6^+$.

The Ar–benzene$^+$ complex has been studied spectroscopically by Dopfer *et al.*,[19] by Neusser and coworkers,[20,21] and by Meijer and co-workers.[11,22] The first paper concerns the intramolecular C–H stretch modes; the latter four studies involve also the intermolecular or van der Waals modes of the complex. In the present paper we describe a theoretical study of the Ar–benzene$^+$ complex that considers these van der Waals modes and, in particular, the effect of the nonadiabatic Jahn–Teller coupling on these modes. We assumed that the van der Waals modes, because of their very low frequency, may be separated adiabatically from the intramolecular modes of benzene$^+$. The standard treatment of van der Waals complexes implies then that the geometry of the monomers will be frozen, preferably at their vibrationally averaged geometry.[23] In line with the above considerations,[15,17,18] we took this frozen geometry for benzene$^+$ to be of D_{6h} symmetry. The Jahn–Teller effect that we studied is entirely due to the van der Waals forces between the Ar atom and the benzene$^+$ cation, and we believe this investigation to be the first that considers such an intermolecular Jahn–Teller effect in detail. Later, it may be appropriate to include also the coupling between the intra- and intermolecular Jahn–Teller effects.

A phenomenon occurring in open-shell systems that may interfere with the Jahn–Teller effect is spin–orbit coupling. The electronic $^2E_{1g}$ ground state of benzene$^+$, in D_{6h} symmetry, has a substantial electronic orbital angular momentum about the sixfold axis, but it has been known for a long time from EPR (electron paramagnetic resonance) studies[24,25] that spin–orbit coupling is very small. High-resolution optical spectra[26–28] gave an upper bound of 0.01 cm^{-1} for the spin–orbit splittings in C_5H_5 and it is expected that they are of similar small size in benzene$^+$. We therefore neglected spin–orbit coupling in our calculations.

With these assumptions the Ar–benzene$^+$ complex has two adiabatic intermolecular potential surfaces that correlate with the $\tilde{X}\,^2E_{1g}$ ground state of benzene$^+$. These potentials depend on three coordinates: the components (x,y,z) of the vector $\mathbf{R}$ that point from the center of mass of benzene$^+$ to the Ar nucleus. When Ar is on the sixfold symmetry axis of benzene$^+$, which we take as the z axis of our coordinate system, the complex has C_{6v} symmetry, its electronic ground state is degenerate, and the two potentials coincide. This electronic degeneracy leads to a quadratic intermolecular Jahn–Teller coupling with the van der Waals bend or x, y mode of e_1 symmetry. There is no linear coupling because that would require a mode of e_2 symmetry and the only other van der Waals mode, the stretch or z mode, has a_1 symmetry. These van der Waals modes have large amplitudes and they cannot be classified with respect to the C_{6v} point group of the equilibrium geometry. Instead, one may use the permutation-inversion group PI(C_{6v}), also called molecular symmetry group $C_{6v}(M)$,[29] which is isomorphic to the point group in this case. The a_1, e_1, and e_2 symmetry labels of the van der Waals modes refer to the PI group.

For the *ab initio* calculation of the adiabatic potential energy surfaces we applied a special method for cationic complexes[9,10] that is both convenient and efficient. In Sec. II of this paper we describe this calculation, the analytic fit, the scaling procedure to ensure the correct long-range behavior, and some characteristics of the two potentials. In Sec. III we treat the nonadiabatic coupling and diabatization of the potential, and in Sec. IV the nuclear motion problem on the coupled diabatic potential surfaces. The results, vibronic energy levels, wave functions, and some simulated spectra, are discussed in Sec. V. In Sec. VI we present the conclusions.

II. ADIABATIC POTENTIAL SURFACES

A. *Ab initio* calculations

The intermolecular potential surfaces of the Ar–benzene$^+$ complex were computed by a special method that we developed for cationic (open-shell) complexes,[9] which we call the IP method. This IP method implies that the interaction energy of a cationic complex A–B$^+$ is calculated as the sum of the interaction energy $E_{\rm int}^{(0)}$ of the neutral (closed-shell) complex A–B and a quantity $\Delta_{\rm int}$ that is the difference

$$\Delta_{\rm int} = I_{\rm AB} - I_{\rm B} \tag{1}$$

between the ionization energy of the complex A–B and the ionization energy of monomer B. The (geometry-dependent) ionization energies $I_{\rm AB}$ and $I_{\rm B}$ can be efficiently computed by the outer valence Green's function (OVGF) method.[30] The IP method was tested on the Rg–CO$^+$ complexes with Rg=He, Ne, Ar[9] and on the He–HF$^+$ complex[10] by comparison with direct calculations of the interaction energy of the ionic complexes by the RCCSD(T) method, a partially spin-restricted version of the CCSD(T) method developed[31,32] for open-shell systems. The main contribution to the geometry-dependent part of the ionization energy $I_{\rm AB}$ is the induction energy due to the polarization of monomer A by the charge and multipole moments of B$^+$. In the tests on Rg–CO$^+$ and He–HF$^+$, it turned out that the interaction energy of A–B$^+$ obtained from the IP method is quite accurate in the short range, but much less accurate for the long-range induction energy. Apparently, the OVGF method is not sufficiently accurate to represent the correlation effects in the properties of the interacting subsystems, at long range. The relevant properties here are the polarizability of A and the multipole moments of B$^+$. It is easy to compute these monomer properties at a high level of electron correlation and to scale the long-

Downloaded 11 Feb 2013 to 131.174.248.95. Redistribution subject to AIP license or copyright; see http://jcp.aip.org/about/rights_and_permissions

range coefficients in the induction energy that contain these properties. This scaling implies that the coefficients obtained in an analytic fit of the long-range induction energy computed by the IP method are replaced by the corresponding values obtained from accurate monomer polarizabilities and multipole moments. With this scaling, the interaction potentials given by the IP method agree with the RCCSD(T) values to within a few percent for all distances.[9,10] Also, unscaled versions of the IP method have been applied,[33–35] however. As was shown[10] on the example of He–HF^+, the method can also be applied to open-shell monomers with degenerate electronic states, $HF^+(X\,^2\Pi)$ in this case, to obtain multiple asymptotically degenerate potential surfaces. The two potentials in this example correspond to electronic states of the complex with A' and A'' symmetry. All one needs to do in such cases is to compute not only the first but also higher ionization energies of the complex A–B. For the Ar–benzene$^+$ complex two asymptotically degenerate potential surfaces are required that correlate with the $^2E_{1g}$ ground state of benzene$^+$.

In most ionic complexes the binding is much stronger than in the corresponding neutral complexes and the equilibrium intermolecular separation is considerably smaller. This implies that one needs to know the potential of the neutral complex for very small intermolecular distances, in order to obtain a complete potential surface of the ionic complex by the IP method. In the Introduction we already mentioned that the interaction in Ar–benzene$^+$ is not much stronger than the interaction in the neutral Ar–benzene complex, however, and that the equilibrium distances are not very different. Another problem that may occur is that the geometry of the monomer that is ionized changes drastically upon ionization. The geometry of benzene$^+$ is very similar to the geometry of neutral benzene,[18] so we avoid this complication. Finally, we were fortunate because the interaction energy of neutral Ar–benzene is accurately known from CCSD(T) calculations by Koch *et al.*[6] The potential energy surface obtained from these calculations was tested by a computation of the frequencies of the van der Waals modes of the Ar–benzene complex and a comparison with experiment,[4,5] and was found to be very accurate indeed. Hence, we already know the potential $E_{\rm int}^{(0)}$ and we need to compute only the quantity $\Delta_{\rm int}$, i.e., the ionization energies of Ar–benzene and benzene, to obtain the intermolecular potentials of Ar–benzene$^+$.

The first and second ionization energy of Ar-benzene and the ionization energy of benzene that yield $\Delta_{\rm int}^{(1)}$ and $\Delta_{\rm int}^{(2)}$ were computed by the OVGF method with the program GAUSSIAN 98.[36] The geometry of the benzene molecule was chosen to be the same as used by Koch *et al.* to compute the neutral interaction energy, with nearest neighbor C–C and C–H distances of 1.397 and 1.080 Å, respectively. In the dynamical calculations (see below), benzene$^+$ is frozen at the ground state geometry with D_{6h} symmetry; hence, the intermolecular potential depends only on the Cartesian components (x,y,z) of the vector **R** that points from the nuclear center of mass of benzene$^+$ to the Ar nucleus. The xy plane is the plane of the benzene$^+$ monomer and the x axis bisects the vector between two neighboring carbon atoms. Sometimes we find it convenient to express the vector **R** in polar coordinates: the length R, the angle θ between **R** and the z axis and the angle ϕ between the projection of **R** onto the xy plane and the x axis. The ionization energy of the complex was corrected for the basis set superposition error by means of the Boys–Bernardi counterpoise procedure.

TABLE I. Convergence of $\Delta_{\rm int}^{(1)}$ from the first ionization energy and of the total Ar–benzene$^+$ interaction energy (in cm^{-1}) with a basis set: DZ is short for cc-PVDZ, TZ for cc-PVTZ, first is the basis on benzene, second on Ar. The interaction energy $E_{\rm int}^{(0)}$ of neutral Ar–benzene was computed with the potential of Koch *et al.* (Ref. 6). All calculations at $(\theta,\phi)=(0,0)$. I_B is the ionization energy of C_6H_6 in eV; the experimental value is 9.25 eV.

Basis	DZ/DZ	DZ/TZ	DZ/aug-DZ	DZ/aug-TZ	aug-DZ/aug-DZ
I_B	9.037	9.039	9.052	9.054	9.207
$R=2.5$ Å					
$\Delta_{\rm int}^{(1)}$	−696.14	−638.42	−773.30	−762.59	−743.81
$E_{\rm int}^{(0)}+\Delta_{\rm int}^{(1)}$	5165.75	5223.47	5088.59	5099.30	5118.08
$R=3.5$ Å					
$\Delta_{\rm int}^{(1)}$	−125.13	−96.76	−111.98	−101.79	−97.40
$E_{\rm int}^{(0)}+\Delta_{\rm int}^{(1)}$	−509.38	−481.01	−496.23	−486.04	−481.65
$R=5$ Å					
$\Delta_{\rm int}^{(1)}$	−20.71	−34.71	−45.81	−49.04	−47.02
$E_{\rm int}^{(0)}+\Delta_{\rm int}^{(1)}$	−116.29	−130.29	−141.39	−144.62	−142.60

Ionization energies $I_{\rm AB}$ were computed for a series of geometries with $R=2.5$, 3, 3.5, 4, 5, 6 Å, $\theta=0°$, 10°, 20°, 30°, 45°, 60°, and $\phi=0°$, 15°, 30°. Additional computations were made in the range of the van der Waals minimum for $R=3.2$, 3.4, 3.6, 3.7, 3.8 Å with the same θ values as above and $\phi=0$, and for $R=2$ and 4.5 Å with $\theta=\phi=0$. Long-range computations were performed for $R=10$, 12, 14, 16 Å and $\theta=0$, 30, 60, 90°, with $\phi=0$ only, because the ϕ dependence of the long-range energy was found to be extremely weak.

Several (augmented) correlation consistent polarized valence n-zeta (aug-cc-PVnZ) basis sets from Refs. 37, 38 with $n=2$ and 3 were tested for the computation of the ionization energies; see Table I. The largest is an aug-cc-PVDZ basis on both Ar and benzene. The ionization energy of benzene computed in this basis is close to the experimental value: the difference is only 0.04 eV. Ionization energies computed in the smaller bases are always about 0.15 eV lower, but the quantity $\Delta_{\rm int}=I_{\rm AB}-I_{\rm B}$ is clearly not as sensitive to the basis. The nonaugmented bases yield reasonable results at small to intermediate separations but fail for large R, with an underestimate of the attraction by 30%–50%. Augmentation of the Ar basis yields much better results in the long range, the difference in $\Delta_{\rm int}$ with the computation in the largest basis being only 4%. This can be understood as it is the polarization of the Ar atom that yields the dominant geometry-dependent (induction) contribution to $\Delta_{\rm int}$ and augmentation of the basis is required to obtain accurate polarizabilities. Use of an aug-cc-PVTZ basis for Ar yields slightly better results at small and intermediate separations. Computations in the largest basis were almost an order of magnitude more expensive and we therefore performed all computations in the aug-cc-PVTZ basis on Ar and the cc-PVDZ basis on benzene.

Downloaded 11 Feb 2013 to 131.174.248.95. Redistribution subject to AIP license or copyright; see http://jcp.aip.org/about/rights_and_permissions

B. Analytic fit of the potentials

The neutral Ar–benzene complex is a typical van der Waals molecule bound by dispersion forces. The long-range dispersion attraction decays as R^{-6} with increasing intermolecular distance R. The potential of Koch *et al.*[6] that we use as the $E_{\rm int}^{(0)}$ term in the potential of the Ar–benzene$^+$ complex is very accurate in the region of the van der Waals well, but it was represented by an analytic model involving Morse potentials that decay exponentially with R. Since the long-range behavior of the potential may play a role in the bound levels of the ionic complex we decided to make a new fit of the potential of Koch *et al.* with slightly different analytic functions that involve R^{-6} terms. First we used the potential of Koch *et al.* to compute 2551 interaction energy values on a grid of points (x,y,z) within the range of their *ab initio* computed points, as reported in Ref. 6. These energies were then fit to a functional form that has the correct asymptotic behavior. This functional form is largely identical to that of Koch *et al.*, who used the many-body expansion

$$E_{\rm int}^{(0)}(x,y,z)=W_0\Bigg(\sum_k V_2(r_k)+\sum_{l<k} V_3(r_k,r_l) + \sum_{m<l<k} V_4(r_k,r_l,r_m)\Bigg), \tag{2}$$

where

$$r_k=[(x-X_k)^2+(y-Y_k)^2+b_z(z-Z_k)^2]^{1/2} \tag{3}$$

is a modified distance between the Ar atom and the kth carbon atom located at (X_k,Y_k,Z_k), while b_z and W_0 are fit parameters. The two-body contribution was taken by Koch *et al.* to be a Morse-type expansion,

$$V_2(r_k)=w^2(r_k)+\sum_{i=3}^{5} c_i w^i(r_k)+c_6\tilde{w}^6(r_k), \tag{4}$$

with

$$w(r_k)=1-\exp[-a(r_k-r_0)], \tag{5}$$

and $\tilde{w}(r_k)=w(r_k)$ for $r_k\geqslant r_0$ and 0 for $r_k<r_0$. Also, c_i with $i=3,...,6$, a, and r_0 are fit parameters. Our modification implies that we chose

$$w(r_k)=\frac{g}{\tilde{r}_k^3}-\exp[-a(r_k-r_0)], \tag{6}$$

with the additional fit parameter g, where $\tilde{r}_k$ is the distance between the Ar atom and the kth carbon atom. This ensures that our potential decays as R^{-6}. Following Koch *et al.*, the three-body contributions are

$$V_3(r_k,r_l)=\sum_{i=1}^{4} c_{ii}w^i(r_k)w^i(r_l)+\sum_{i<j}^{4} c_{ij}[w^i(r_k)w^j(r_l) + w^j(r_k)w^i(r_l)], \tag{7}$$

and the four-body terms are represented by an analogous sum of triple products of w functions. A total of 24 linear and 4 nonlinear parameters were used in the fit. The potential surface that we obtained from this refit is equal to the potential of Ref. 6 to within a few tenths of a percent (less than 1 cm^{-1}) in the region of the van der Waals well. In the region with R larger than 6 Å (the interaction energy of neutral Ar–benzene is about -30 cm^{-1} at $R=6$ Å), our potential decays slower than the potential of Koch *et al.* and the difference becomes larger, of course. The fit of Koch *et al.* oscillates in this region and adopts positive values, while our fit is probably still reliable. The interaction energy of the ionic complex in this long range region is dominated by the induction energy contained in the quantity $\Delta_{\rm int}$, hence, the accuracy of the neutral potential $E_{\rm int}^{(0)}$ is not so critical. However, its correct behavior is.

In order to obtain the two asymptotically degenerate potentials $V^{(1)}(\mathbf{R})$ and $V^{(2)}(\mathbf{R})$ of the ionic complex, we first attempted to fit $\Delta_{\rm int}^{(1)}$ and $\Delta_{\rm int}^{(2)}$ separately. We found, however, that a fit of the sum $E_{\rm int}^{(0)}+\Delta_{\rm int}^{(i)}$ for $i=1$, 2 leads to better results. Since we know that the van der Waals well of the ionic complex is not very different from that of neutral Ar–benzene and the functional form used by Koch *et al.* was very successful in describing the potential surface of the latter complex (except for the asymptotics) we used this form also for a fit of the two adiabatic potential surfaces of Ar–benzene$^+$. Explicit long-range interaction terms were now added, however, and we ensured that the potentials $V^{(1)}(\mathbf{R})$ and $V^{(2)}(\mathbf{R})$ coincide when the Ar atom is on the z axis by writing

$$\begin{aligned} V^{(1)}(\mathbf{R})&=S(\mathbf{R})+\frac{1}{2}P_{2,1}(\theta)D(\mathbf{R})+L(\mathbf{R}),\\ V^{(2)}(\mathbf{R})&=S(\mathbf{R})-\frac{1}{2}P_{2,1}(\theta)D(\mathbf{R})+L(\mathbf{R}), \end{aligned} \tag{8}$$

where $P_{2,1}(\theta)$ is an associated Legendre function $P_{l,m}$ with $l=2$ and $m=1$ that equals zero for $\theta=0$. Note that the choice of $P_{2,1}(\theta)$ to make the difference potential $V^{(1)}(\mathbf{R})-V^{(2)}(\mathbf{R})$ vanish for $\theta=0$ does not imply that this difference potential indeed behaves as $P_{2,1}(\theta)$ when Ar is displaced from the z axis. We will see below that it actually behaves as a quadratic function of $\sin\theta$ or, since $P_{2,1}(\theta)$ is linear in $\sin\theta$ for small θ, that the function $D(\mathbf{R})$ is also linear in $\sin\theta$ for small values of θ. The functions $S(\mathbf{R})$ and $D(\mathbf{R})$ were written in the same form as Eq. (2) with $w(r_k)$ given by Eq. (5), as we now have separate long-range terms $L(\mathbf{R})$ that ensure the correct asymptotic behavior. These long-range terms are expressed in polar coordinates,

$$L(R,\theta)=\sum_{n=4}^{10}\sum_{l=0}^{n-4} C_{n,l}P_l(\cos\theta)R^{-n}D_n(\beta R), \tag{9}$$

where $P_l(\cos\theta)$ are Legendre polynomials and $D_n(\beta R)$ are Tang–Toennies damping functions.[39] Only terms with even values of n and l occur in this expansion, because of the D_{6h} symmetry of benzene$^+$ and the spherical symmetry of the Ar atom. The expansion does not contain the angle ϕ because it was found that the potentials in the long range are very nearly independent of ϕ. The ionization energy calculations were not sufficiently accurate to differentiate between $V^{(1)}(\mathbf{R})$ and $V^{(2)}(\mathbf{R})$ for $R>10$ Å. The long-range behavior of both potentials is therefore determined by the same function $L(R,\theta)$. In order to obtain the long-range expansion

Downloaded 11 Feb 2013 to 131.174.248.95. Redistribution subject to AIP license or copyright; see http://jcp.aip.org/about/rights_and_permissions

coefficients $C_{n,l}$ the energies computed for $R \geqslant 10$ Å were fit to the functional form of Eq. (9) with the damping functions $D_n(\beta R)$ set equal to 1. The error in this long-range fit is on the order of 2%. The parameters in the functions used to fit $S(\mathbf{R})$ and $D(\mathbf{R})$ and the parameter β in the damping functions $D_n(\beta R)$ were obtained from a subsequent least squares fit of the data for $R < 10$ Å. The error in the fit of the sum potential $S(\mathbf{R}) + L(\mathbf{R})$ is smaller than 1%, except for geometries where the potential becomes zero and the relative error is larger (but the absolute error remains small). Even for the much smaller difference potential containing the functions $D(\mathbf{R})$, the fit is quite accurate, typically 2%–3%.

The scaling of the long-range induction energy required to obtain accurate potentials for ionic complexes from the IP method[9,10] requires the coefficients $C_{n,l}$ in Eq. (9) in terms of monomer properties: the charge and multipole moments of $C_6H_6^+$ and the polarizability of Ar. These properties, and the induction coefficients $C_{n,l}$ in which they occur, were computed with the POLCOR suite of codes.[40] Multipole moments considered are the charge $Q=1$, quadrupole, hexadecapole, and 64-pole. The isotropic term containing $C_{4,0}$ is the only contribution, which is due purely to induction effects, the higher coefficients $C_{n,l}$ with $n=6$, 8, and 10 in the fit of Eq. (9) contain induction as well as dispersion contributions that cannot be separated. It is therefore appropriate to scale only $C_{4,0}$. In previous work[9,10] we scaled also $C_{5,1}$ but this coefficient is zero in the present case. The polarizability of Ar obtained from the fitted coefficient $C_{4,0}$, $8.63\,a_0^3$, is significantly lower than the accurate value of $11.08\,a_0^3$ and $C_{4,0}$ was therefore scaled by the ratio 11.08/8.63.

C. Characteristics of the potentials

Figure 1 shows contour plots of the scaled potential surfaces $V^{(1)}(\mathbf{R})$ and $V^{(2)}(\mathbf{R})$. It is clear from these plots that the two potentials have a joint minimum with Ar on the z axis and $R_e = 3.506$ Å. The dissociation energy D_e equals 520 cm^{-1}. In agreement with experiment,[11] the binding is not much stronger than in neutral Ar–benzene with $D_e = 387\,\mathrm{cm}^{-1}$ and the equilibrium distance R_e is not much smaller ($R_e = 3.555$ Å for the neutral complex). The scaling, of course, affected these values, but did not alter the characteristics of the potential very much: without scaling D_e would have been 484 cm^{-1} and $R_e = 3.514$ Å. The well depth and R_e value of the scaled potential are in good agreement with the experimental data of Ref. 11, hence we are confident that the IP method with the scaling of the long-range induction coefficient worked well in this case also.

An interesting difference is observed when the Ar atom is displaced from the minimum in the x or y (bending) direction. The higher one of the two potentials, $V^{(2)}(\mathbf{R})$, is about equally steep in this direction as the potential of neutral Ar–benzene, but the lower one, $V^{(1)}(\mathbf{R})$, is surprisingly flat. This was quite unexpected, as one would think that the ionic complex would be more rigid than the neutral complex. We will see below that the fundamental bending frequency of Ar–benzene$^+$, when calculated on the adiabatic potential $V^{(2)}(\mathbf{R})$, is about equal to that of neutral Ar–benzene, but considerably lower on $V^{(1)}(\mathbf{R})$. Nonadiabatic coupling must be taken into account, however, and the two potential surfaces cannot be used independently in dynamical calculations. Still, we expect the zero-point energy of Ar–benzene$^+$ to be considerably lower than that of Ar–benzene. We will see below that the lower zero-point energy and the increase of D_e from 387 to 520 cm^{-1} upon ionization of the Ar–benzene complex agree well with the stabilization energy of 170 cm^{-1} derived from the observed ionization energies, so that we may indeed conclude that our Ar–benzene$^+$ potentials are accurate.

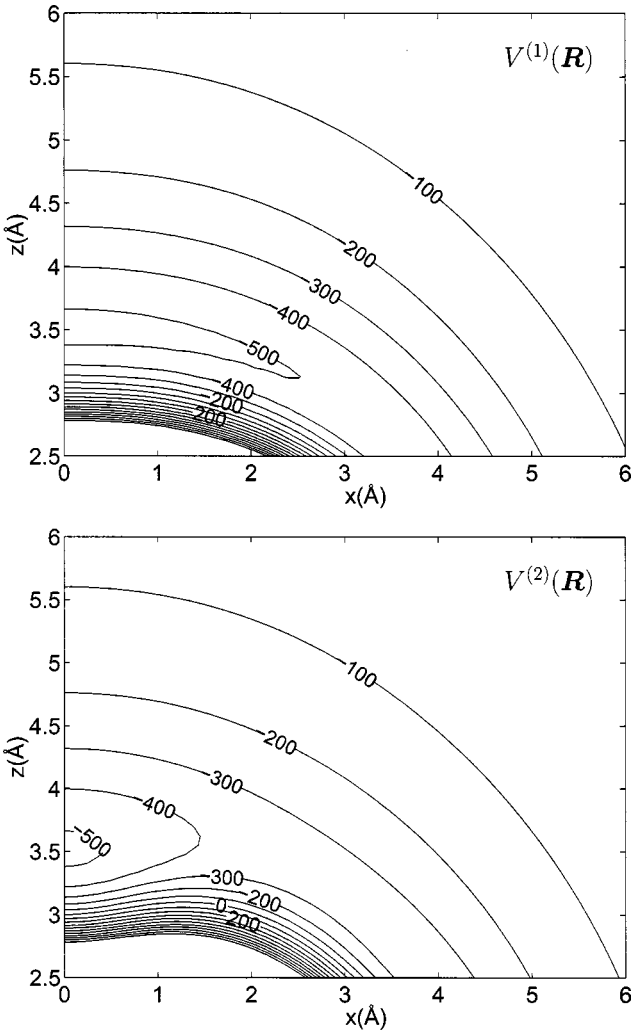

FIG. 1. Adiabatic potentials $V^{(1)}(\mathbf{R})$ and $V^{(2)}(\mathbf{R})$ in cm^{-1}; cuts in the xz plane ($y=0$).

When we analyze the splitting of the two potentials more closely, we find that it is very nearly a quadratic function of $\rho = \sqrt{x^2+y^2} = R \sin\theta$. One observes this more globally in Fig. 2, for $R = 3.5$ Å near the minimum, and especially for somewhat smaller R, where the lower surface has a local maximum and the higher one has still a minimum. This confirms the occurrence of a quadratic Jahn–Teller effect by vibronic coupling of the electronic E_{1g} ground state, twofold degenerate for $x=y=0$, to the bending (x,y) mode of e_1 symmetry. Only modes of e_2 symmetry would cause linear Jahn–Teller coupling,[17] but there are no fundamentals of this symmetry among the van der Waals modes. The dependence

Downloaded 11 Feb 2013 to 131.174.248.95. Redistribution subject to AIP license or copyright; see http://jcp.aip.org/about/rights_and_permissions

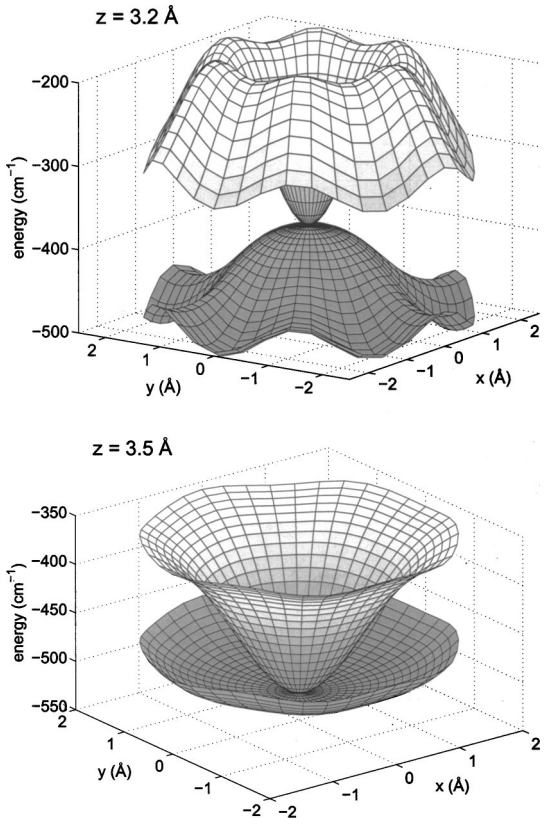

FIG. 2. Behavior of adiabatic potentials $V^{(1)}(\mathbf{R})$ and $V^{(2)}(\mathbf{R})$ near the z axis, for $z=3.2$ Å and for the equilibrium height $z=3.5$ Å.

on ϕ is rather weak for both potentials and even smaller for the difference potential.

Finally, we might comment on why the induction energy in the ionic complex does not lead to stronger binding. The reason is that the strong attraction proportional to R^{-4} from the charge-induced dipole interaction is largely canceled by the interaction of the dipole induced on Ar with the permanent quadrupole of benzene$^+$. This interaction is repulsive when Ar is on the z axis and proportional to R^{-6} and it takes away a significant amount of binding for R values near the minimum.

We also used the IP method to compute the intermolecular potentials of Ar–benzene$^+$ for excited states of the complex that correlate with the twofold degenerate $\tilde{B}\,^2E_{2g}$ state and the nondegenerate $\tilde{C}\,^2A_{2u}$ state of benzene$^+$, which are both about 3 eV above the ground state. The two asymptotically degenerate potentials for the E_2 state of the complex are very nearly the same, very similar in shape to the potential of neutral Ar–benzene, and only slightly deeper than the latter. In these states the electron is removed from the highest σ molecular orbital (MO) of benzene. The potential of the A_2 state shows a much deeper well, with D_e about three times larger than for neutral Ar–benzene, and the much smaller R_e value of 2.89 Å that one would expect for an ionic complex. In this A_2 state the electron is removed from the lowest π MO of benzene, which is equally distributed over the six carbon atoms. Apparently this reduces the steric repulsion with the Ar atom. These excited state potentials will not be further discussed, however.

III. NONADIABATIC COUPLING AND DIABATIZATION

The nuclear kinetic energy operator for the relative motion of Ar and benzene$^+$ and the overall rotation of the complex is[1]

$$T^{\mathrm{nuc}}=\frac{1}{2}(\mathbf{J}-\mathbf{l})\mathbf{I}^{-1}(\mathbf{J}-\mathbf{l})+\frac{p_R^2}{2\mu_{\mathrm{AB}}}, \tag{10}$$

where $\mathbf{p}_R$ is the linear momentum conjugate to the coordinate $\mathbf{R}$ and $\mathbf{l}=\mathbf{R}\times\mathbf{p}_R$ is the angular momentum of Ar relative to benzene$^+$. The reduced mass μ_{AB} is given by $\mu_{\mathrm{AB}}^{-1}=m_{\mathrm{Ar}}^{-1}+m_{\mathrm{benzene}^+}^{-1}$. The operator $\mathbf{J}$ is the overall angular momentum of the rotating complex and $\mathbf{I}$ is the inertia tensor of (rigid) benzene$^+$. We take $\mathbf{I}^{-1}$ to be a diagonal matrix with the rotational constants A, $B(=A)$, and C of $C_6H_6^+$ or $C_6D_6^+$ on the diagonal. The total angular momentum $\mathbf{J}$ does not include the electron spin as spin–orbit coupling may be neglected.[24–26] We only considered the rotationless states with $J=0$ in this paper.

In the Born–Oppenheimer or adiabatic approximation one computes the eigenstates $\chi(\mathbf{R})$ of a nuclear motion Hamiltonian that is the sum of this operator T^{nuc} and one of the two adiabatic potentials $V^{(1)}(\mathbf{R})$ and $V^{(2)}(\mathbf{R})$. Important nonadiabatic coupling occurs, however. The term with p_R^2 in the nuclear kinetic energy operator, when expressed in polar coordinates, contains the operator

$$T_\phi=\frac{-\hbar^2}{2\mu_{\mathrm{AB}}R^2\sin^2\theta}\frac{\partial^2}{\partial\phi^2}, \tag{11}$$

which leads to nonadiabatic coupling terms

$$F_{12}=\frac{-\hbar^2}{2\mu_{\mathrm{AB}}R^2\sin^2\theta}\left\langle\Psi_1^{\mathrm{adiab}}\left|\frac{\partial}{\partial\phi}\Psi_2^{\mathrm{adiab}}\right\rangle\frac{\partial}{\partial\phi}\right. \tag{12}$$

and

$$G_{12}=\frac{-\hbar^2}{2\mu_{\mathrm{AB}}R^2\sin^2\theta}\left\langle\Psi_1^{\mathrm{adiab}}\left|\frac{\partial^2}{\partial\phi^2}\Psi_2^{\mathrm{adiab}}\right\rangle\right., \tag{13}$$

between the two adiabatic electronic states Ψ_1^{adiab} and Ψ_2^{adiab} that are degenerate for $\theta=0$. It is clear from these expressions that these coupling matrix elements become singular at $\theta=0$ for all R.

Rather than taking the singular nonadiabatic coupling into account explicitly we constructed a diabatic model with states Φ_1^{diab} and Φ_2^{diab} that removes (or, at least, strongly reduces) the kinetic coupling. A so-called ''crude'' diabatic model[41] would be to construct diabatic states that do not depend on ϕ by using for all values of $\mathbf{R}$ the eigenstates of the electronic Hamiltonian calculated for a fixed nuclear geometry $\mathbf{R}_0$. We propose a similar diabatic model, but we only fix the coordinate ϕ to $\phi_0=0$, while R and θ adopt the values corresponding to the actual geometry considered. In the electronic $\tilde{X}\,^2E_{1g}$ ground state of benzene$^+$ that is considered here, the electron is removed from one of the two degenerate highest occupied π MO's of benzene. These MO's each have a single nodal plane perpendicular to the plane of the molecule. For a canonical set of MO's these nodal planes coincide with orthogonal σ_v and σ_d reflection symmetry planes: σ_v is the yz plane; σ_d the xz plane. These

Downloaded 11 Feb 2013 to 131.174.248.95. Redistribution subject to AIP license or copyright; see http://jcp.aip.org/about/rights_and_permissions

two MO's, and the corresponding many-electron states of benzene$^+$, are degenerate and they may be freely mixed. Each MO keeps a single nodal surface perpendicular to the plane of the molecule; the mixing rotates these surfaces about the z axis. This is also what seems to happen for the adiabatic states of the Ar–benzene$^+$ complex when $\theta>0$ and the Ar atom rotates around the z axis over the angle ϕ. An increase of ϕ by 60° is equivalent to a cyclic (simultaneous) permutation of the carbon and hydrogen nuclei in the benzene$^+$ monomer. From the PI(C_{6v}) symmetry of the complex it follows that the adiabatic states stay equivalent under this permutation and that their wave functions are simply obtained from the original wave functions by mixing the substates 1 and 2. For functions of E_1 symmetry, as we have here, the angle $\Delta\alpha$ in the rotation matrix:

$$\mathbb{R}(\Delta\alpha)=\begin{pmatrix}\cos\Delta\alpha & -\sin\Delta\alpha\\ \sin\Delta\alpha & \cos\Delta\alpha\end{pmatrix}, \tag{14}$$

which mixes the adiabatic wave functions is equal to $\Delta\phi=60°$. Also, when ϕ is changed into $-\phi$ or $180°-\phi$ the adiabatic wave functions stay equivalent. The transformation matrix is an improper rotation (with determinant -1) in that case. For arbitrary changes $\Delta\phi$ the adiabatic states are not simply related by mixing them, but our model assumes that they are and that the mixing angle $\Delta\alpha$ is equal to $\Delta\phi$. We assume, in other words, that the adiabatic states of Ar–benzene$^+$ simply ''follow'' the Ar atom.

The most general transformation between two adiabatic and diabatic states can be written as

$$(\Psi_1^{\text{adiab}}\Psi_2^{\text{adiab}})=(\Phi_1^{\text{diab}}\Phi_2^{\text{diab}})\mathbb{R}(\alpha(\mathbf{R})), \tag{15}$$

with a mixing angle $\alpha(\mathbf{R})$ that depends on the nuclear coordinates $\mathbf{R}$. The diabatic states in our model are defined in terms of the (calculated) adiabatic states by Eq. (15) with the general mixing angle $\alpha(\mathbf{R})$ equal to the geometrical angle ϕ. If the model were exact, these diabatic states would be ϕ independent and equal to the adiabatic states calculated for $\phi=0$, with R and θ given by their ''real'' values. It is not difficult to prove, when the (orthonormal) diabatic states are indeed ϕ independent, that the matrix element $\langle\Psi_1^{\text{adiab}}|(\partial/\partial\phi)\Psi_2^{\text{adiab}}\rangle$ in the nonadiabatic coupling parameter F_{12} of Eq. (12) should be exactly equal to unity.

In order to check our model, we calculated this nonadiabatic coupling matrix element from the adiabatic states computed by the program MOLPRO,[42] as a function of the geometry $\mathbf{R}$. The electronic structure method used is the CAS-SCF (complete interacting space self-consistent field) method with the five π electrons of benzene$^+$ in the active space spanned by the six π MO's. We used a two-state-averaged version of CAS-SCF, which correctly reproduces the twofold degeneracy of the ground state for $\theta=0$. The derivative matrix element $\langle\Psi_1^{\text{adiab}}|(\partial/\partial\phi)\Psi_2^{\text{adiab}}\rangle$ in Eq. (12) was computed by numerical differentiation (a feature of MOLPRO) with step size $\Delta\phi=1°$ for a range of ϕ values from 0 to 30°. Different (aug-)cc-PVnZ basis sets from Refs. 37, 38 were used, but the results were essentially the same. They are shown in Fig. 3 for an augmented double zeta basis ($n=2$).

It is clear from this figure that the nonadiabatic coupling matrix element is very nearly equal to 1 indeed, especially when the Ar atom is close to the z axis. That is the most important region, since the couplings F_{12} and G_{12} between the adiabatic states become singular in this region and the diabatic states should be truly ϕ independent there, in order to remove this kinetic coupling. Even when the Ar atom

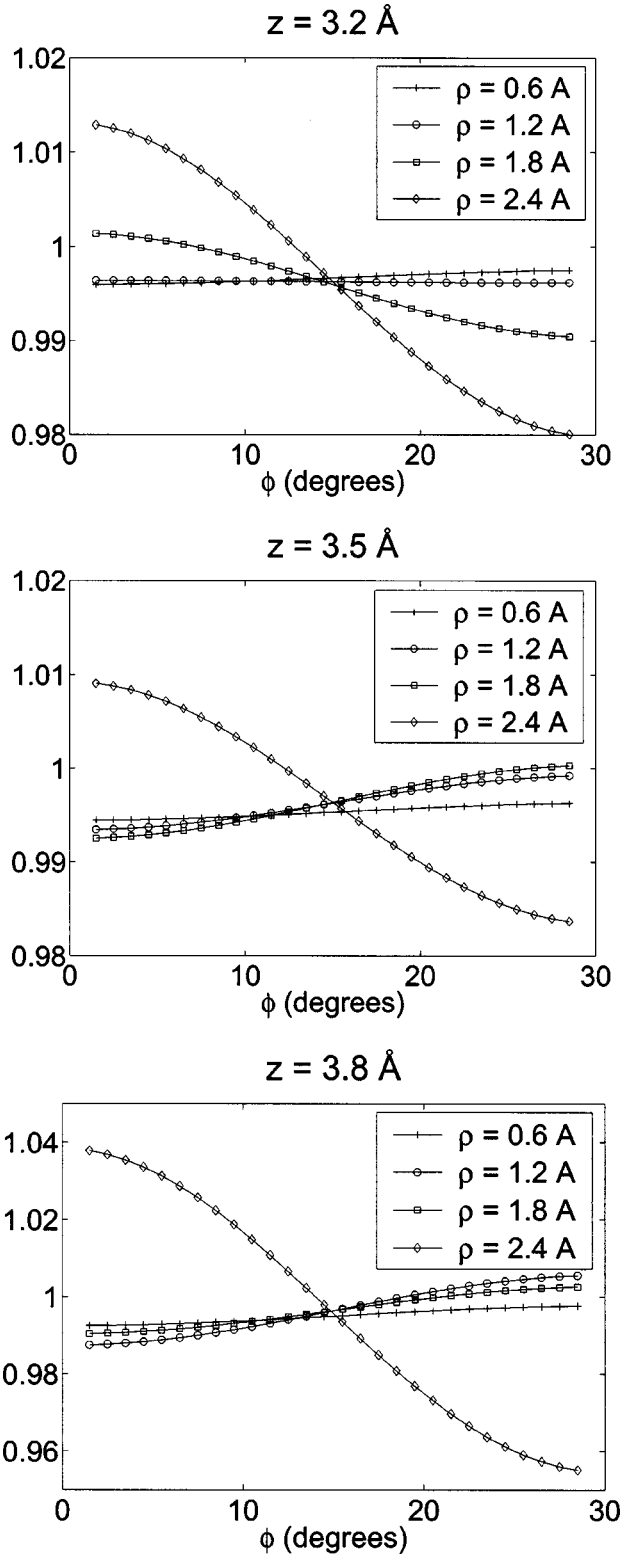

FIG. 3. Nonadiabatic coupling matrix element $\langle\Psi_1^{\text{adiab}}|(\partial/\partial\phi)\Psi_2^{\text{adiab}}\rangle$ as a function of the azimuthal angle ϕ for different values of z and $\rho=\sqrt{x^2+y^2}$.

Downloaded 11 Feb 2013 to 131.174.248.95. Redistribution subject to AIP license or copyright; see http://jcp.aip.org/about/rights_and_permissions

moves as far as 2.4 Å away from the z axis, i.e., over the hydrogen atoms, the coupling matrix element does not differ from 1 by more than 4%. So, our diabatic model works extremely well and is globally valid. The reasons for this are the near-cylindrical symmetry of benzene$^+$ and the fact that the states Ψ_1^{adiab} and Ψ_2^{adiab} are only coupled by the operator $\partial/\partial\phi$.

The diabatic states are not eigenstates of the electronic Hamiltonian, so they are coupled in the nuclear motion problem by the potential energy operator. From the transformation formula in Eq. (15) with $\alpha(\mathbf{R})=\phi$, it follows that the diabatic potentials are

$$V_{11}^{\text{diab}}(\mathbf{R})=\frac{1}{2}[V^{(1)}(\mathbf{R})+V^{(2)}(\mathbf{R})]+\frac{\cos 2\phi}{2}\times[V^{(1)}(\mathbf{R})-V^{(2)}(\mathbf{R})],$$
$$V_{22}^{\text{diab}}(\mathbf{R})=\frac{1}{2}[V^{(1)}(\mathbf{R})+V^{(2)}(\mathbf{R})]-\frac{\cos 2\phi}{2}\times[V^{(1)}(\mathbf{R})-V^{(2)}(\mathbf{R})], \quad (16)$$
$$V_{12}^{\text{diab}}(\mathbf{R})=\frac{\sin 2\phi}{2}[V^{(2)}(\mathbf{R})-V^{(1)}(\mathbf{R})].$$

Finally, let us note that the idea that the electron hole in the highest occupied π MO's of benzene$^+$ follows the Ar atom provides also a qualitative explanation of the shape of the adiabatic potential surfaces $V^{(1)}(\mathbf{R})$ and $V^{(2)}(\mathbf{R})$. The lower surface $V^{(1)}(\mathbf{R})$, see Fig. 1, is very flat in the x, y directions, as if in substate 1 the electron hole makes space for the Ar atom when it moves away from the z axis. The hole can easily do that when it chooses among the degenerate MO's the one that points toward the Ar atom. The upper surface $V^{(2)}(\mathbf{R})$ is quite similar in shape to the potential surface of neutral Ar–benzene, as if the Ar atom does not feel that an electron was removed from the benzene molecule. This seems to imply that in adiabatic substate 2 the electron hole chooses the MO that has its nodal plane (nearly) through the Ar nucleus.

IV. VIBRONIC MODEL

The two-state vibronic model used in our calculations is based on the Hamiltonian

$$\mathbb{H}=\begin{pmatrix} T^{\text{nuc}} & 0 \\ 0 & T^{\text{nuc}} \end{pmatrix}+\begin{pmatrix} V_{11}^{\text{diab}}(\mathbf{R}) & V_{12}^{\text{diab}}(\mathbf{R}) \\ V_{12}^{\text{diab}}(\mathbf{R}) & V_{22}^{\text{diab}}(\mathbf{R}) \end{pmatrix}, \quad (17)$$

with the nuclear kinetic energy operator T^{nuc} given by Eq. (10) and diabatic potentials $V_{ij}^{\text{diab}}(\mathbf{R})$ obtained from the *ab initio* computed adiabatic potentials $V^{(1)}(\mathbf{R})$ and $V^{(2)}(\mathbf{R})$ through Eq. (16). The off-diagonal kinetic energy operator F_{12} is neglected because it is very small in the diabatic basis. This is easily shown by writing the coupling matrix element $\langle\Phi_1^{\text{diab}}|(\partial/\partial\phi)\Phi_2^{\text{diab}}\rangle$ in the diabatic basis, substituting Eq. (15) with $\alpha(\mathbf{R})=\phi$, and using the property that expectation values of the real anti-hermitian operator $\partial/\partial\phi$ over real wave functions are zero. Then, if we assume that $\langle\Psi_1^{\text{adiab}}|(\partial/\partial\phi)\Psi_2^{\text{adiab}}\rangle=1$ in the adiabatic basis (which is very nearly true; see Fig. 3) we find that $F_{12}=0$ in the diabatic basis. The second-order coupling G_{12} is expected to be very small as well and is neglected too.

The solutions of the two-state vibronic model are

$$\Psi(\mathbf{r}_{\text{el}},\mathbf{R})=\Phi_1^{\text{diab}}\chi_1(\mathbf{R})+\Phi_2^{\text{diab}}\chi_2(\mathbf{R})$$
$$=\Psi_1^{\text{adiab}}[\chi_1(\mathbf{R})\cos\phi+\chi_2(\mathbf{R})\sin\phi]$$
$$+\Psi_2^{\text{adiab}}[-\chi_1(\mathbf{R})\sin\phi+\chi_2(\mathbf{R})\cos\phi], \quad (18)$$

with $\mathbf{r}_{\text{el}}$ denoting the electronic coordinates. They include, in particular, the quadratic Jahn–Teller effect of the bend van der Waals mode of symmetry e_1. Especially this bend mode has a large amplitude and is strongly anharmonic. The electronic wave functions $\Phi_1^{\text{diab}}(\mathbf{r}_{\text{el}},\mathbf{R})$ and $\Phi_2^{\text{diab}}(\mathbf{r}_{\text{el}},\mathbf{R})$ were not explicitly considered in the calculation of the vibronic levels; they entered through the diabatic potentials $V_{ij}^{\text{diab}}(\mathbf{R})$ in Eq. (17). The nuclear wave functions $\chi_1(\mathbf{R})$ and $\chi_2(\mathbf{R})$ in Eq. (18) were expanded in a basis of three-dimensional harmonic oscillator functions,[1,2]

$$H_k(x-x_e)H_l(y-y_e)H'_m(z-z_e), \quad (19)$$

centered at $(x_e,y_e,z_e)=(0,0,R_e=3.506\ \text{Å})$. The functions $H_k(x-x_e)$ and $H_l(y-y_e)$ were taken from the same set, i.e., $k_{\max}=l_{\max}$, and they were restricted to $k+l\leqslant k_{\max}$ in order to make the basis invariant under C_{6v} symmetry operations. The functions $H'_m(z-z_e)$ were taken from a different set. The matrix elements of the diabatic potentials in this basis were computed numerically with a $32\times32\times32$ points Gauss–Hermite quadrature.[43] The matrix elements of the nuclear kinetic energy operator, Eq. (10), were obtained analytically with the aid of harmonic oscillator step up and step down operators. The vibronic problem was solved variationally, by diagonalization of the matrix $\mathbb{H}$ of Eq. (17) in the given basis.

A high-order basis ($k_{\max}=l_{\max}=18$ and $m_{\max}=15$) and a basis size of 2565 were needed to simultaneously converge both functions $\chi_1(\mathbf{R})$ and $\chi_2(\mathbf{R})$. The nonlinear parameters in the basis are the harmonic frequencies ω_e; they were optimized in calculations with smaller basis sets by minimization of the ground vibronic level, while considering also some of the excited levels. We took an ω_e value of 2.5 cm^{-1} for the functions $H_k(x-x_e)$ and $H_l(y-y_e)$ and of 40 cm^{-1} for the functions $H'_m(z-z_e)$. By comparison with calculations in smaller $12\times12\times10$ and $15\times15\times12$ basis sets, we estimate that the lower levels have converged to within a few hundredths of cm^{-1}, while some of the higher combination levels may still shift by several tenths of cm^{-1}.

The mass of the Ar atom is 39.950 u, the masses of $C_6H_6^+$ and $C_6D_6^+$ are 78.047 and 84.084 u, respectively. For the rotational constants we took the recent experimental values[18] $A=B=0.187\,06\ \text{cm}^{-1}$, $C=0.093\,445\ \text{cm}^{-1}$ for $C_6H_6^+$ and $A=B=0.154\,52\ \text{cm}^{-1}$, $C=0.077\,253\ \text{cm}^{-1}$ for $C_6D_6^+$.

V. RESULTS AND DISCUSSION

Before we discuss the results of the vibronic calculations we present in Tables II and III, the van der Waals levels calculated on the separate adiabatic potentials $V^{(1)}(\mathbf{R})$ and

Downloaded 11 Feb 2013 to 131.174.248.95. Redistribution subject to AIP license or copyright; see http://jcp.aip.org/about/rights_and_permissions

TABLE II. van der Waals modes calculated on the adiabatic potential surface $V^{(1)}(\mathbf{R})$. The energy is relative to the zero-point level with $D_0=486.19\ \mathrm{cm}^{-1}$. The mode character is given in terms of (x,y) bend b and (z) stretch s quanta. Root mean square displacements are defined as $\Delta x=[\langle x^2\rangle-\langle x\rangle^2]^{1/2}$, etc. For the e_1 and e_2 modes Δx and Δy are reversed in the second substate. Line strengths in units of the model described in the text; perpendicular refers to the sum of x and y components, parallel to the z component.

Energy (cm^{-1})	mode	PI(C_{6v}) symmetry	Δx (Å)	Δy (Å)	$\langle z\rangle$ (Å)	Δz (Å)	Line strength	
							Perpendicular	Parallel
0.00		a_1	0.572	0.572	3.506	0.124		
8.96	b^1	e_1	1.002	0.579	3.475	0.134	2.337 14	0.0
16.89	b^2	a_1	1.000	1.000	3.439	0.148	0.0	0.025 01
17.72	b^2	e_2	1.085	0.942	3.437	0.145	0.0	0.0
24.27	b^3	b_2	1.230	1.230	3.380	0.162	0.0	0.0
25.04	b^3	e_1	1.439	0.837	3.394	0.167	0.002 14	0.0
29.47	b^3	b_1	1.077	1.077	3.431	0.141	0.0	0.0
31.51		e_2	1.611	1.032	3.337	0.186	0.0	0.0
32.32		a_1	1.333	1.333	3.343	0.191	0.0	0.002 16
38.31		b_2	1.469	1.469	3.292	0.208	0.0	0.0
38.82		e_1	1.754	1.069	3.298	0.213	0.000 04	0.0
38.93		e_2	1.395	0.960	3.403	0.149	0.0	0.0
46.10		e_2	1.824	1.128	3.272	0.227	0.0	0.0
46.54		a_1	1.491	1.491	3.282	0.232	0.0	0.005 26
48.23		e_1	1.332	1.325	3.366	0.159	0.000 16	0.0
48.62		b_1	1.283	1.283	3.381	0.162	0.0	0.0
49.10	s^1	a_1	0.566	0.566	3.565	0.215	0.0	0.833 88
53.84		b_2	1.563	1.563	3.252	0.240	0.0	0.0
54.22		e_1	1.861	1.121	3.264	0.244	0.000 02	0.0
56.46	b^6	a_2	1.462	1.462	3.320	0.166	0.0	0.0
57.88		e_2	1.667	1.061	3.346	0.176	0.0	0.0
58.88		a_1	1.396	1.396	3.352	0.172	0.0	0.001 51
59.96	b^1s^1	e_1	0.977	0.631	3.533	0.228	0.003 34	0.0

$V^{(2)}(\mathbf{R})$. The first potential is very flat in the (x,y) bend direction and, indeed, the bend fundamental b^1 has the very low frequency of 9 cm^{-1}. This is quite surprising for a cationic complex, as the corresponding frequency of the neutral Ar–benzene complex is 33 cm^{-1}.[5] We observe in Table II that the amplitude of the ground state van der Waals vibrations in the x and y directions is nearly twice as large as in the neutral complex,[2] while the amplitude in the z direction is of the same size as in neutral Ar–benzene. The second potential is similar in shape to that of neutral Ar–benzene and the van der Waals modes on this potential are also similar, both in frequency and amplitude; cf. Ref. 5. The stretch frequency of 49 cm^{-1} on the potential $V^{(1)}(\mathbf{R})$ is somewhat higher than the value of 42 cm^{-1} on the potential $V^{(2)}(\mathbf{R})$, which may be related to Fermi resonance-type interactions with the bending overtones. The first overtone b^2 is higher in frequency than s^1 for $V^{(2)}(\mathbf{R})$ and may push the stretch frequency down, while the potential $V^{(1)}(\mathbf{R})$ has several bend overtones of a_1 symmetry below the stretch frequency that may push the latter up. Line strengths, discussed below, confirm this picture.

Table IV shows the results of the two-state vibronic calculations. The ground state is twofold degenerate (E_1 symmetry) and is dominated (88%) by a nodeless vibrational

TABLE III. Van der Waals modes calculated on the adiabatic potential surface $V^{(2)}(\mathbf{R})$. Zero-point level with $D_0=460.66\ \mathrm{cm}^{-1}$. For explanations, see Table II.

Energy (cm^{-1})	mode	PI(C_{6v}) symmetry	Δx (Å)	Δy (Å)	$\langle z\rangle$ (Å)	Δz (Å)	Line strength	
							Perpendicular	Parallel
0.00		a_1	0.303	0.303	3.551	0.117		
32.43	b^1	e_1	0.550	0.317	3.569	0.119	0.650 22	0.0
42.17	s^1	a_1	0.390	0.390	3.602	0.189	0.0	0.594 85
62.33	b^2	e_2	0.581	0.579	3.585	0.122	0.0	0.0
65.23	b^2	a_1	0.546	0.546	3.593	0.146	0.0	0.185 99
70.12	b^1s^1	e_1	0.703	0.406	3.612	0.178	0.005 36	0.0
81.67	s^2	a_1	0.500	0.500	3.651	0.238	0.0	0.000 36
89.46	b^3	b_2	0.712	0.712	3.598	0.125	0.0	0.0
89.76	b^3	b_1	0.708	0.708	3.599	0.125	0.0	0.0
94.80	b^3	e_1	0.827	0.477	3.613	0.165	0.000 32	0.0
95.67		e_2	0.747	0.737	3.618	0.169	0.0	0.0
98.54		a_1	0.705	0.705	3.630	0.199	0.0	0.009 16

Downloaded 11 Feb 2013 to 131.174.248.95. Redistribution subject to AIP license or copyright; see http://jcp.aip.org/about/rights_and_permissions

TABLE IV. Vibronic levels of Ar–$C_6H_6^+$. Zero-point level with $D_0=478.47\ cm^{-1}$. Column 2 lists the symmetry of the vibrational components, column 3 the total vibronic symmetry. Columns 4 and 5 list the occupations of the two vibrational components (with reversed values for the second E_1 and E_2 substate). For further explanations, see Table II.

Energy	Symmetry		Occupation		Δx	Δy	$\langle z\rangle$	Δz	Line strength	
(cm^{-1})	vib	total	1	2	(Å)	(Å)	(Å)	(Å)	Perp	Paral
0.00	a_1+e_2	E_1	0.88	0.12	0.783	0.474	3.502	0.130		
1.25	e_1	A_1	0.50	0.50	0.818	0.818	3.475	0.134	1.391 21	0.0
10.12	$e_1+b_1+b_2$	E_2	0.54	0.46	1.020	0.897	3.452	0.145	1.474 77	0.0
12.56	a_1+e_2	E_1	0.83	0.17	1.205	0.709	3.443	0.155	0.0	0.004 71
16.95	e_2	B_2	0.50	0.50	1.210	1.210	3.387	0.163	0.0	0.0
17.41	e_1	A_1	0.50	0.50	1.172	1.172	3.397	0.167	0.041 96	0.0
21.74	e_2	B_1	0.50	0.50	1.046	1.046	3.440	0.142	0.0	0.0
22.78	$e_1+b_1+b_2$	E_2	0.64	0.36	1.519	0.973	3.364	0.188	0.015 94	0.0
26.09	a_1+e_2	E_1	0.78	0.22	1.626	0.967	3.342	0.198	0.0	0.000 03
30.35	e_2	B_2	0.50	0.50	1.421	1.421	3.312	0.210	0.0	0.0
30.46	$e_1+b_1+b_2$	E_2	0.65	0.35	1.345	0.942	3.413	0.153	0.000 07	0.0
31.65	e_1	A_1	0.50	0.50	1.460	1.460	3.295	0.214	0.001 57	0.0
36.04	$e_1+b_1+b_2$	E_2	0.69	0.31	1.757	1.086	3.295	0.227	0.000 90	0.0
38.56	a_1+e_2	E_1	0.65	0.35	1.515	1.177	3.346	0.202	0.0	0.000 62
39.66	e_2	B_1	0.50	0.50	1.225	1.225	3.400	0.163	0.0	0.0
41.79	a_1+e_2	E_1	0.61	0.39	1.635	1.236	3.310	0.208	0.0	0.000 01
45.10	e_2	B_2	0.50	0.50	1.501	1.501	3.280	0.242	0.0	0.0
46.70	e_1	A_1	0.50	0.50	1.498	1.498	3.284	0.240	0.000 19	0.0
47.78	$e_1+b_1+b_2$	E_2	0.68	0.32	1.531	1.127	3.360	0.193	0.000 02	0.0
47.87	a_1+e_2	E_1	0.92	0.08	0.687	0.477	3.568	0.217	0.0	0.049 00
48.70	e_1	A_2	0.50	0.50	1.454	1.454	3.324	0.168	0.000 19	0.0
50.24	e_1	A_2	0.50	0.50	0.450	0.450	3.570	0.120	0.055 04	0.0
50.39	e_1	A_1	0.50	0.50	1.270	1.270	3.400	0.222	0.001 14	0.0
51.88	$e_1+b_1+b_2$	E_2	0.68	0.32	1.758	1.220	3.280	0.242	0.0	0.0
53.37	e_1	A_1	0.50	0.50	1.030	1.030	3.476	0.231	0.003 06	0.0
56.06	a_1+e_2	E_1	0.61	0.39	1.554	1.402	3.306	0.220	0.0	0.000 50
57.02	e_2	B_1	0.50	0.50	1.410	1.410	3.344	0.194	0.0	0.0
58.26	a_1+e_2	E_1	0.54	0.46	1.492	1.484	3.313	0.212	0.0	0.000 29

wave function; see Fig. 4. In contrast with neutral Ar–benzene, where the vibrational ground state wave function has a_1 symmetry and is nearly cylindrical about the z axis,[2] the dominant vibrational component in the ground state here is not purely a_1. It is clearly biased in the x (or, for the other substate, y) direction by admixture of an e_2 vibration (x^2-y^2). The minor vibrational component (12%) is purely $e_2(xy)$. This is a consequence of the fact that the electronic charge distribution in each of the two degenerate (E_1) substates of the cationic complex is not sixfold symmetric. In our diabatic representation of these substates the electron hole occurs in the π-MO with the xz plane as the nodal plane in one of the substates; in the other one it occurs in the π-MO with the yz plane as the nodal plane.

The lowest excited state in Table IV has A_1 symmetry and a remarkably low frequency: 1.25 cm^{-1}. An analysis of its wave function, see Fig. 5, shows clearly that it is a bending (x,y) mode of vibrational symmetry e_1. Next, at 10.12 cm^{-1}, we find a vibronic state of E_2 symmetry that has mostly e_1 bend character as well; see Fig. 6. Theoretical considerations of the quadratic Jahn–Teller effect (equivalent to a Renner–Teller effect) predict that the bend mode of e_1 symmetry in combination with the degenerate electronic state of E_1 symmetry produces three vibronic levels: nondegenerate levels of A_1 and A_2 symmetry and a twofold degenerate level of E_2 symmetry. Two of these levels have now

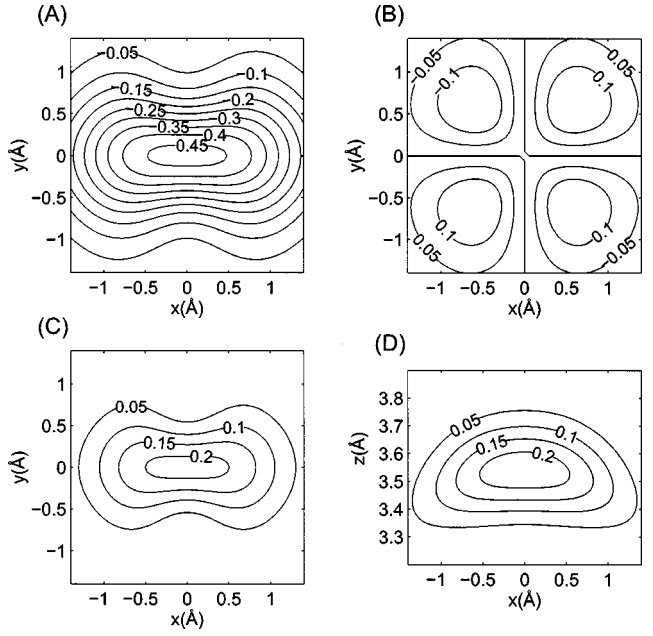

FIG. 4. Ground state vibronic wave function, E_1 symmetry. Cuts (x,y) at $z=3.5$ Å through the two vibrational components (with contributions of a_1 and e_2 symmetry) are shown in panels (a) and (b), while panel (c) shows the total density. Panel (d) shows a (x,z) cut at $y=0$ through the total density. One of the two degenerate substates is displayed, the other one is equivalent, with the vibrational components interchanged and rotated over 90° about the z axis.

Downloaded 11 Feb 2013 to 131.174.248.95. Redistribution subject to AIP license or copyright; see http://jcp.aip.org/about/rights_and_permissions

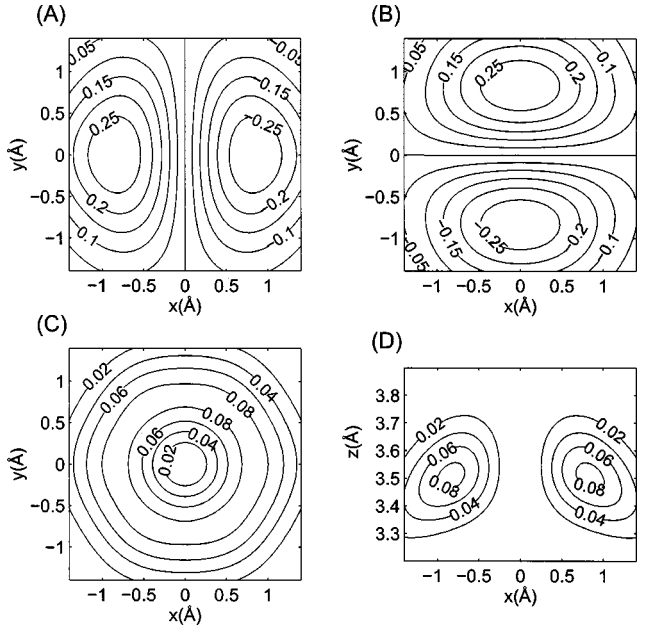

FIG. 5. Vibronic state of A_1 symmetry at 1.25 cm^{-1}. Cuts (x,y) at $z=3.5$ Å through the two vibrational components (of e_1 symmetry) are shown in panels (a) and (b), panel (c) shows the total density. Panel (d) shows a (x,z) cut at $y=0$ through the total density.

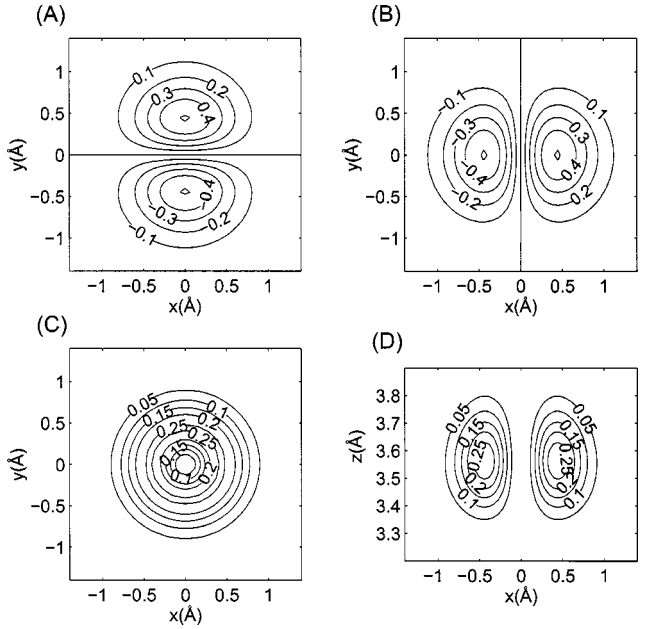

FIG. 7. Vibronic state of A_2 symmetry at 50.24 cm^{-1}. Cuts (x,y) at $z=3.5$ Å through the two vibrational components (of e_1 symmetry) are shown in panels (a) and (b), panel (c) shows the total density. Panel (d) shows a (x,z) cut at $y=0$ through the total density.

been identified for the bend fundamental, b^1. The third one of A_2 symmetry is found at 50.24 cm^{-1}. Both by its vibronic wave function, shown in Fig. 7, and by the remarkably small root mean square displacements in the x and y directions, see Table IV, it can be clearly distinguished among the many levels of a more complex nature found at this higher energy. This analysis reveals that even in the absence of a linear Jahn–Teller effect, the splitting of the (quadratically) Jahn–Teller active van der Waals bend mode is quite dramatic. In the separate adiabatic potentials, i.e., when nonadiabatic coupling is neglected, the bend fundamental has a frequency of 9 or 32 cm^{-1}. In the two-state vibronic model it splits into three vibronic states at 1, 10, and 50 cm^{-1}.

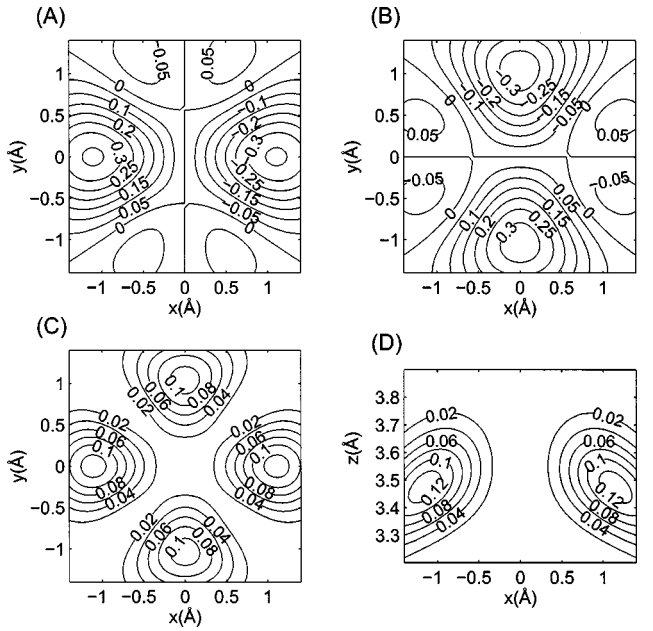

FIG. 6. Vibronic state of E_2 symmetry at 10.12 cm^{-1}. Cuts (x,y) at $z=3.5$ Å through the two vibrational components (with contributions of e_1, b_1, and b_2 symmetry) are shown in panels (a) and (b), while panel (c) shows the total density. Panel (d) shows a (x,z) cut at $y=0$ through the total density. One of the two degenerate substates is displayed, the other one is equivalent, with the total density rotated over 45° about the z axis.

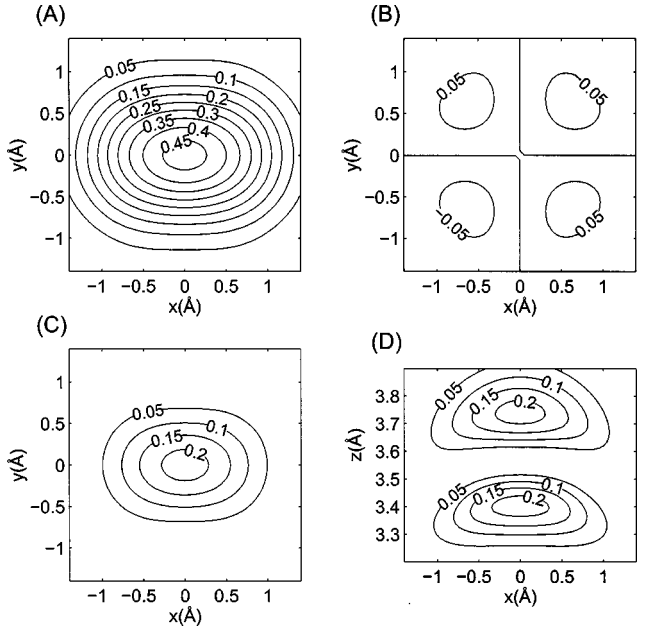

FIG. 8. Vibronic state of E_1 symmetry at 47.87 cm^{-1} that corresponds to the stretch fundamental s^1. Cuts (x,y) at $z=3.75$ Å through the two vibrational components (with contributions of a_1 and e_2 symmetry) are shown in panels (a) and (b), while panel (c) shows the total density. Panel (d) shows a (x,z) cut at $y=0$ through the total density. One of the two degenerate substates is displayed, the other one is equivalent and rotated over 90° about the z axis.

Downloaded 11 Feb 2013 to 131.174.248.95. Redistribution subject to AIP license or copyright; see http://jcp.aip.org/about/rights_and_permissions

TABLE V. Vibronic levels of $Ar–C_6D_6^+$. Zero-point level with $D_0=480.10\,cm^{-1}$. For explanations, see Table IV.

Energy (cm^{-1})	Symmetry		Occupation		Δx (Å)	Δy (Å)	$\langle z\rangle$ (Å)	Δz (Å)	Line strength	
	vib	total	1	2					Perp	Paral
0.00	a_1+e_2	E_1	0.88	0.12	0.763	0.461	3.504	0.127		
1.07	e_1	A_1	0.50	0.50	0.794	0.794	3.479	0.131	1.320 62	0.0
9.24	$e_1+b_1+b_2$	E_2	0.54	0.46	0.990	0.874	3.456	0.140	1.402 14	0.0
11.55	a_1+e_2	E_1	0.84	0.16	1.169	0.688	3.449	0.149	0.0	0.004 38
15.51	e_2	B_2	0.50	0.50	1.176	1.176	3.396	0.156	0.0	0.0
16.05	e_1	A_1	0.50	0.50	1.141	1.141	3.404	0.161	0.043 66	0.0
19.73	e_2	B_1	0.50	0.50	1.019	1.019	3.445	0.138	0.0	0.0
20.97	$e_1+b_1+b_2$	E_2	0.64	0.36	1.485	0.947	3.372	0.181	0.013 70	0.0
24.04	a_1+e_2	E_1	0.78	0.22	1.591	0.947	3.350	0.191	0.0	0.000 04
27.76	$e_1+b_1+b_2$	E_2	0.65	0.35	1.310	0.908	3.420	0.147	0.000 07	0.0
27.91	e_2	B_2	0.50	0.50	1.394	1.394	3.321	0.203	0.0	0.0
29.15	e_1	A_1	0.50	0.50	1.437	1.437	3.303	0.208	0.001 65	0.0
33.11	$e_1+b_1+b_2$	E_2	0.69	0.31	1.736	1.066	3.301	0.222	0.000 77	0.0
35.24	a_1+e_2	E_1	0.64	0.36	1.464	1.159	3.356	0.192	0.0	0.000 26
36.46	e_2	B_1	0.50	0.50	1.191	1.191	3.406	0.158	0.0	0.0
38.20	a_1+e_2	E_1	0.61	0.39	1.631	1.207	3.312	0.207	0.0	0.000 01
41.24	e_2	B_2	0.50	0.50	1.485	1.485	3.283	0.238	0.0	0.0
42.78	e_1	A_1	0.50	0.50	1.482	1.482	3.287	0.236	0.000 18	0.0
43.95	$e_1+b_1+b_2$	E_2	0.67	0.33	1.487	1.114	3.366	0.190	0.000 04	0.0
44.28	e_1	A_2	0.50	0.50	1.413	1.413	3.336	0.160	0.000 18	0.0
46.65	e_1	A_1	0.50	0.50	1.371	1.371	3.355	0.187	0.000 08	0.0
46.94	a_1+e_2	E_1	0.90	0.10	0.702	0.493	3.562	0.217	0.0	0.046 81
46.95	e_1	A_2	0.50	0.50	0.430	0.430	3.567	0.118	0.049 53	0.0
47.40	$e_1+b_1+b_2$	E_2	0.68	0.32	1.738	1.206	3.284	0.239	0.000 00	0.0
51.03	e_1	A_1	0.50	0.50	0.809	0.809	3.532	0.222	0.002 72	0.0
51.37	a_1+e_2	E_1	0.62	0.38	1.522	1.368	3.315	0.220	0.0	0.001 42
52.62	e_2	B_1	0.50	0.50	1.379	1.379	3.351	0.189	0.0	0.0
53.36	a_1+e_2	E_1	0.54	0.46	1.487	1.461	3.311	0.203	0.0	0.000 15

Most of the higher levels involve bend overtones: b^2 (vibrational symmetry a_1+e_2), $b^3(e_1+b_1+b_2)$, $b^4(a_1+2e_2)$, etc. The lowest level of total symmetry A_2 (vibrational symmetry e_1) at 48.70 cm^{-1} is clearly a b^5 overtone, but in most cases the mode character is less clear. Another exception is the level of E_1 symmetry at 47.87 cm^{-1} that corresponds (mostly) to the van der Waals stretch fundamental vibration, s^1, of a_1 symmetry. The wave function of this vibronic state in Fig. 8 confirms this assignment.

The vibronic levels of the perdeuterated complex $Ar–C_6D_6^+$ are listed in Table V. They are quite similar in nature to those of $Ar–C_6H_6^+$. The vibronic levels corresponding to the bend fundamental occur at 1.07, 9.24, and 46.95 cm^{-1} and to the stretch fundamental at 46.94 cm^{-1}. The isotope shifts are typically what one might expect from the change in the reduced mass of the complex (for the stretch frequency) and the change in the rotational constants of the benzene cation (for the bend); cf. the analysis for neutral Ar–benzene in Ref. 5.

The first direct comparison to experimental data concerns the binding energy D_0 of the complex. It was mentioned above that $D_e=519.87\,cm^{-1}$ in our potential, and it was anticipated that the zero-point vibrational energy in Ar–benzene$^+$ will be lower than in neutral Ar–benzene because one of the two adiabatic potentials is much flatter in the (x,y) bend direction than the potential of the neutral complex. The full vibronic calculations show that this is true. The zero-point energy is 41.4 cm^{-1}, while it is 59 cm^{-1} for neutral Ar–benzene.[6] This is mostly an effect of the flatter potential indeed: the zero-point energy calculated on the separate adiabatic potential $V^{(1)}$ is 33.7 cm^{-1} and on the adiabatic potential $V^{(2)}$ it is 59.2 cm^{-1}. But we could not anticipate that the zero-point energy of 41.4 cm^{-1} in the vibronic calculation is even lower than the average zero-point energy on the two adiabatic potentials. The binding energy from the full vibronic calculation is $D_0=478.47\,cm^{-1}$. Deuteration of the complex gives $D_0=480.10\,cm^{-1}$, a lowering of the zero-point energy, from 41.4 to 39.8 cm^{-1}. This value of D_0 for $Ar–C_6D_6^+$ agrees well with the experimental upper bound of 485 cm^{-1}.[11] Hence, we may conclude that the well depth of our (adiabatic) potentials for Ar–benzene$^+$ is reliable. The difference in D_0 with the neutral complex, 150 cm^{-1} according to our calculations, is somewhat smaller than the experimental difference of 170 cm^{-1} obtained from the redshift of the ionization energy of benzene upon complexation with Ar.[12] The potential of Koch *et al.*[6] that we used in the construction of our potentials for the cationic complex, see Sec. II, is too deep by about 15 cm^{-1}[11] and the fact that D_0 agrees better with experiment for Ar–benzene$^+$ than for neutral Ar–benzene is fortuitous.

Also, the frequencies of the van der Waals modes in $Ar–C_6H_6^+$ and $Ar–C_6D_6^+$ have been measured.[11,20–22] The vibronic levels from our calculations are quite dense, and in order to help with the assignment of the experimental spectra we constructed a model dipole function, calculated transition

Downloaded 11 Feb 2013 to 131.174.248.95. Redistribution subject to AIP license or copyright; see http://jcp.aip.org/about/rights_and_permissions

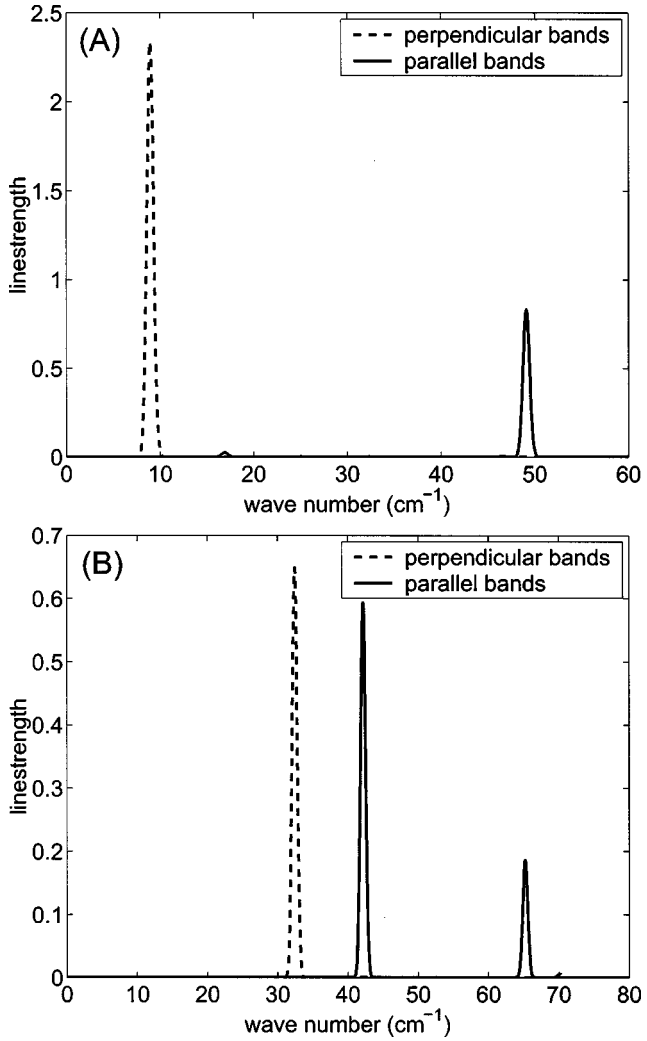

FIG. 9. Simulated far-infrared spectra of $Ar–C_6H_6^+$ on adiabatic potentials $V^{(1)}(\mathbf{R})$ [panel (a)] and $V^{(2)}(\mathbf{R})$ [panel (b)]. Line strength in units of model described in the text.

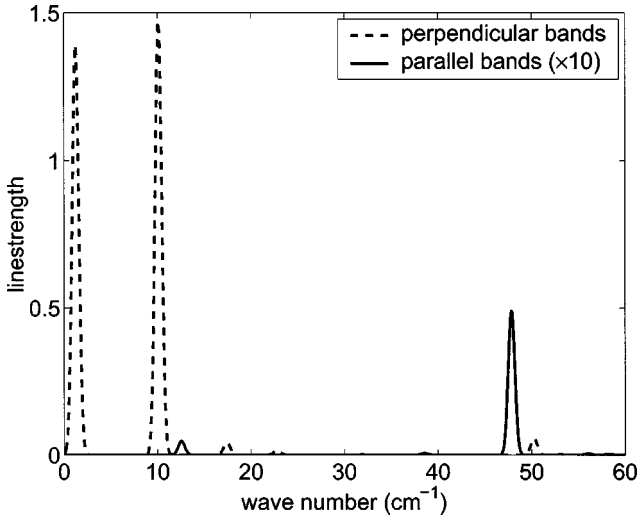

FIG. 10. Simulated far-infrared spectrum of $Ar–C_6H_6^+$ from the full vibronic model. Line strength in units of the model described in the text.

strengths, and simulated the far-infrared spectrum. An obvious contribution to the dipole moment function of the complex is due to the motion of the charged benzene$^+$ monomer relative to the center of mass of the complex. This produces a dipole moment vector $\boldsymbol{\mu}$ that depends linearly on the position vector $\mathbf{R}=(x,y,z)$ of Ar relative to benzene$^+$, with a proportionality factor of $m_{\mathrm{Ar}}/(m_{\mathrm{Ar}}+m_{\mathrm{benzene}^+})$. Further dipole contributions are due to the polarization of Ar by the benzene cation and to other interaction-induced effects. The spectra measured are infrared spectra[11,22] due to combination bands of the van der Waals modes with some of the intramolecular modes of the benzene cation, or they were obtained by selectively exciting the van der Waals excited states of the cationic complex[20] or the corresponding Rydberg series of the neutral complex[21] by a resonance-enhanced two-photon process. The actual dependence of the dipole function on the Ar position vector $\mathbf{R}$ is more complicated, but we simply assumed a dipole linear in (x,y,z) with a proportionality constant of one. With this dipole function we calculated the dipole transition strengths between the ground state of E_1 symmetry and each of the excited vibronic states that originate from the van der Waals modes. This quantity was averaged over the two substates of the degenerate ground state and summed over the excited substates when the excited state is degenerate as well. The parallel line strength is the transition strength calculated with the z component of the dipole, the perpendicular line strength is a sum over the x and y transition strengths. The simulated far-infrared spectrum was generated with the use of the calculated transition frequencies and line strengths, convoluted with a Gaussian lineshape of full width half-maximum (FWHM) 0.83 cm^{-1}. The spectra in Fig. 9 were produced with the vibrational states from separate calculations on the two adiabatic potentials. The spectrum in Fig. 10 was generated by using the vibronic states from the full calculation, with the assumption that the effective dipole moment function for the van der Waals modes does not depend on the electronic coordinates. The justification of the latter assumption is that the effective vibrational dipole moment function is an expectation value (or transition matrix element) over the electronic wave functions.

The spectra in Fig. 9 obtained from the levels computed on the adiabatic potentials $V^{(1)}(\mathbf{R})$ and $V^{(2)}(\mathbf{R})$ show the features that one might expect for anharmonic vibrations. The bend mode gives rise to a perpendicular line at frequencies of 9 and 32 cm^{-1} for $V^{(1)}(\mathbf{R})$ and $V^{(2)}(\mathbf{R})$, respectively, and the stretch mode to a parallel line at frequencies of 49 and 42 cm^{-1}. Weaker parallel lines at 17 and 64 cm^{-1} in the first and second spectrum, respectively, correspond to the bend overtone of a_1 symmetry; also see Tables II and III. The line in the second spectrum is relatively stronger because of mixing (Fermi resonance) between the bend overtone b^2 and the stretch fundamental s^1. The vibronic spectrum in Fig. 10 shows unexpected features, however. Most striking is that the very low excited state at 1.3 cm^{-1} that is one of the Jahn–Teller split vibronic states originating from the bend mode causes a strong perpendicular absorption line. It is almost equally strong as the perpendicular line at 10.1 cm^{-1} that corresponds to another one of these vibronic states of the bend mode. Also, the third bend state at 50.2 cm^{-1} is visible as a perpendicular line in the simulated spectrum, but

Downloaded 11 Feb 2013 to 131.174.248.95. Redistribution subject to AIP license or copyright; see http://jcp.aip.org/about/rights_and_permissions

much weaker. The vibronic transition corresponding to the stretch mode gives rise to a parallel line at 47.9 cm^{-1}, which is relatively much weaker than in the separate adiabatic calculations shown in Fig. 9, although we used the same dipole function. Even weaker lines, both perpendicular and parallel, can be seen in Fig. 10 at 12.6, 17.4, 22.8, 38.6 cm^{-1} and still weaker allowed transitions can be observed in Table IV.

In the experimental spectra of Refs. 20, 21 a line was observed at 48 cm^{-1} and assigned to the stretch vibration. This line agrees very well with our stretch absorption line. In the spectrum of Bakker *et al.*[22] lines were observed at 11, 26, and 46 cm^{-1} as sidebands to the ν_{11} mode of a_{2u} symmetry in D_{6h} and a_1 symmetry in C_{6v}. The line at 46 cm^{-1} was assigned to the stretch mode, previously observed at 48 cm^{-1}.[20,21] From the comparison to our calculations we can conclude that the peak at 11 cm^{-1} must be assigned to one of the vibronic levels that originate from the bend mode, with the unexpectedly low frequency for this mode agreeing very well with our results. The peak observed at 26 cm^{-1} might correspond to the calculated line at 22.8 cm^{-1}. Krause *et al.*[20] also reported a line at 23 cm^{-1}, in agreement with our calculations. Neuhauser *et al.*[21] did not observe this line, however. Krause *et al.* and Neuhauser *et al.* found a peak at 30 cm^{-1}. In our theoretical spectrum we obtained only very weak lines in this region, perhaps because of our model dipole function being too simple. The strong perpendicular line that we predict at 1.3 cm^{-1} could not be observed experimentally since it is too close to the monomer line.[44] All in all, we may conclude that our calculated spectra agree well with the measurements. It is satisfactory, in particular, that the peak at the unexpectedly low frequency of 11 cm^{-1} is clearly explained now.

Bakker *et al.*[22] also measured the van der Waals frequencies of the perdeuterated complex $Ar–C_6D_6^+$. They reported peculiar isotope shifts: instead of the three peaks at 11, 26, and 46 cm^{-1} for $Ar–C_6H_6^+$ they found two peaks at 13 and 34 cm^{-1}. This does not agree with our calculations which predict more usual downward and smaller isotope shifts. It was pointed out[22] that the character of the intramolecular mode to which the van der Waals modes appear as sidebands differs from the corresponding mode in the protonated complex, so that different van der Waals modes may appear as sidebands in the spectrum. We did not find lines with substantial intensity in these regions, however. It is quite surprising also that the stretch mode expected slightly below 48 cm^{-1} is absent from the spectrum of the perdeuterated complex, so one may wonder whether the assignment of these peaks to the van der Waals modes is correct. Another possibility is that the intramolecular Jahn–Teller effect starts playing a role when the benzene$^+$ monomer modes are excited (although the ν_{11} mode is not a Jahn–Teller active mode).

VI. CONCLUSION

Two adiabatic potential energy surfaces $V^{(1)}(\mathbf{R})$ and $V^{(2)}(\mathbf{R})$ for argon interacting with the twofold degenerate $\tilde{X}\,^2E_{1g}$ ground state benzene$^+$ cation were computed by considering the interaction energy of the ionic complex to be the sum of the interaction energy of the neutral complex and the difference in the geometry-dependent ionization energies of the complex and the benzene monomer. The van der Waals minima in these potentials occur for Ar on the C_{6v} symmetry axis of benzene$^+$ (the z axis), where the surfaces coincide. The binding energy D_e of 520 cm^{-1} is only 34% larger than the value for the neutral Ar–benzene complex and the intermolecular separation R_e of 3.506 Å is not much smaller. With these adiabatic potentials we constructed a two-by-two matrix of diabatic potentials from a model based on the assumption that the adiabatic states of the Ar–benzene$^+$ complex geometrically follow the Ar atom. The adiabatic to diabatic mixing angle in this model is the azimuthal angle ϕ of the position vector $\mathbf{R}$ of the Ar atom. The model was checked by *ab initio* calculations of the nonadiabatic $\partial/\partial\phi$ coupling matrix element between the adiabatic states with the two-state-averaged CAS-SCF(5,6) method. It was found to be very accurate. The diabatic potential surfaces were used in solving the Schrödinger equation for the bound vibronic states of the Ar–benzene$^+$ complex with the two diabatic electronic states of E_1 symmetry and a basis of anisotropic three-dimensional harmonic oscillator functions for the van der Waals modes. We studied the effect of isotopic substitution by computing the vibronic levels of both $Ar–C_6H_6^+$ and $Ar–C_6D_6^+$.

A model dipole function was constructed, and the calculated line strengths of transitions starting from the ground vibronic level of E_1 symmetry were used to generate a vibronic far-infrared spectrum. The (quadratically) Jahn–Teller active van der Waals mode is the bend mode of e_1 symmetry that splits into three vibronic states with energies 1.3, 10.1, and 50.2 cm^{-1} and symmetries A_1, E_2, and A_2. The levels at 1.3 and 10.1 cm^{-1} give rise to strong perpendicular absorption lines in the spectrum, the level at 50.2 cm^{-1} to a weaker line, also perpendicular. This very low frequency of the bend mode is quite unexpected for a cationic complex; the van der Waals bend frequency in the neutral Ar–benzene complex is 33 cm^{-1}. It is related to the fact that the lower adiabatic potential $V^{(1)}(\mathbf{R})$ is very flat in the bend (x,y) direction. The bend frequency on this potential in the adiabatic approximation is 9.0 cm^{-1}; on the steeper potential $V^{(2)}(\mathbf{R})$ it is 32.4 cm^{-1}. A strong parallel line in the spectrum at 47.9 cm^{-1} originates from the van der Waals stretch (z) mode, which gives rise to a twofold degenerate vibronic state of E_1 symmetry. This line is substantially weaker than expected from separate calculations on the two potentials in the adiabatic approximation. Several other, weaker, parallel, and perpendicular lines were found as well.

A comparison with the experimental data available[11,20–22] shows good agreement. The binding energy $D_0 = 480\,cm^{-1}$ of the perdeuterated complex agrees well with the experimental upper bound of 485 cm^{-1}.[11] The frequencies of the strong lines at 10.1 cm^{-1} (bend) and 47.9 cm^{-1} (stretch) agree with the measurements, which made it possible to assign the lower peak as a bend mode with unusually low frequency. The assignment of some of the weaker lines is still uncertain, but there are several allowed vibronic transitions in the observed frequency range. The calculated isotope shifts show the behavior that is expected from the change of the reduced mass of the complex and the

Downloaded 11 Feb 2013 to 131.174.248.95. Redistribution subject to AIP license or copyright; see http://jcp.aip.org/about/rights_and_permissions

change of the benzene$^+$ rotational constants, but they do not reflect the surprising change of the van der Waals frequencies that was measured.[22]

ACKNOWLEDGMENTS

We thank Gerard Meijer for the suggestion to study this system, and for a stimulating collaboration. We also thank him and Hans Jürgen Neusser for making available their experimental data. We are grateful to Terry Miller for informing us in detail about the characteristics of aromatic Jahn–Teller systems. Discussions with Gerrit Groenenboom and Paul Wormer were very useful.

[1] A. van der Avoird, J. Chem. Phys. **98**, 5327 (1993).
[2] E. Riedle and A. van der Avoird, J. Chem. Phys. **104**, 882 (1996).
[3] E. Riedle, R. Sussmann, T. Weber, and H. J. Neusser, J. Chem. Phys. **104**, 865 (1996).
[4] W. Kim and P. M. Felker, J. Chem. Phys. **107**, 2193 (1997).
[5] R. Neuhauser, J. Braun, H. J. Neusser, and A. van der Avoird, J. Chem. Phys. **108**, 8408 (1998).
[6] H. Koch, B. Fernández, and J. Makarewicz, J. Chem. Phys. **111**, 198 (1999).
[7] B. Fernández, H. Koch, and J. Makarewicz, J. Chem. Phys. **111**, 5922 (1999).
[8] J. López Cacheiro, B. Fernández, and H. Koch, J. Chem. Phys. **119**, 4762 (2003).
[9] V. F. Lotrich and A. van der Avoird, J. Chem. Phys. **118**, 1110 (2003).
[10] V. F. Lotrich, P. E. S. Wormer, and A. van der Avoird, J. Chem. Phys. **120**, 93 (2004).
[11] R. G. Satink, H. Piest, G. von Helden, and G. Meijer, J. Chem. Phys. **111**, 10750 (1999).
[12] K. Siglow, R. Neuhauser, and H. J. Neusser, J. Chem. Phys. **110**, 5589 (1999).
[13] H. Köppel, L. S. Cederbaum, and W. Domcke, J. Chem. Phys. **89**, 2023 (1988).
[14] J. Eiding, R. Schneider, W. Domcke, H. Köppel, and W. von Niessen, Chem. Phys. Lett. **177**, 345 (1991).
[15] R. Lindner, K. Müller-Dethlefs, E. Wedum, K. Haber, and E. R. Grant, Science **271**, 1698 (1996).
[16] K. Müller-Dethlefs and J. B. Peel, J. Chem. Phys. **111**, 10550 (1999).
[17] B. E. Applegate and T. A. Miller, J. Chem. Phys. **117**, 10654 (2002).
[18] M. Ford, R. Lindner, and K. Müller-Dethlefs, Mol. Phys. **101**, 705 (2003).
[19] O. Dopfer, R. V. Olkhov, and J. P. Maier, J. Chem. Phys. **111**, 10754 (1999).
[20] H. Krause and H. J. Neusser, Chem. Phys. Lett. **213**, 603 (1993).
[21] R. Neuhauser, K. Siglow, and H. Neusser, Phys. Rev. Lett. **80**, 5089 (1998).
[22] J. M. Bakker, R. G. Satink, G. von Helden, and G. Meijer, Phys. Chem. Chem. Phys. **4**, 24 (2002).
[23] M. Jeziorska, P. Jankowski, K. Szalewicz, and B. Jeziorski, J. Chem. Phys. **113**, 2957 (2000).
[24] D. S. McClure, J. Chem. Phys. **20**, 682 (1952).
[25] H. M. McConnell, J. Chem. Phys. **34**, 13 (1961).
[26] L. Yu, S. C. Foster, J. M. Williamson, M. C. Heaven, and T. A. Miller, J. Phys. Chem. **92**, 4263 (1988).
[27] B. E. Applegate, T. A. Miller, and T. A. Barckholtz, J. Chem. Phys. **114**, 4855 (2001).
[28] B. E. Applegate, A. J. Bezant, and T. A. Miller, J. Chem. Phys. **114**, 4869 (2001).
[29] P. R. Bunker and P. Jensen, *Molecular Symmetry and Spectroscopy*, 2nd ed. (NRC Research Press, Ottawa, 1998).
[30] W. von Niessen, J. Schirmer, and L. S. Cederbaum, Comput. Phys. Rep. **1**, 57 (1984).
[31] P. J. Knowles, C. Hampel, and H.-J. Werner, J. Chem. Phys. **99**, 5219 (1993).
[32] P. J. Knowles, C. Hampel, and H.-J. Werner, J. Chem. Phys. **112**, 3106(E) (2000).
[33] K. Ohno, M. Yamazaki, N. Kishimoto, T. Ogawa, and K. Teakeshita, Chem. Phys. Lett. **332**, 167 (2000).
[34] M. Yamazaki, N. Kishimoto, M. Kurita, T. Ogawa, K. Ohno, and K. Teakeshita, J. Electron Spectrosc. Relat. Phenom. **114–116**, 175 (2001).
[35] M. Yamazaki, S. Maeda, N. Kishimoto, and K. Ohno, J. Chem. Phys. **117**, 5707 (2002).
[36] M. J. Frisch, G. W. Trucks, H. B. Schlegel *et al.*, GAUSSIAN 98, Revision A.7, Gaussian, Inc., Pittsburgh, PA, 1998.
[37] T. H. Dunning, J. Chem. Phys. **90**, 1007 (1989).
[38] D. E. Woon and T. H. Dunning, J. Chem. Phys. **100**, 2975 (1994).
[39] K. T. Tang and J. P. Toennies, J. Chem. Phys. **80**, 3726 (1984).
[40] P. E. S. Wormer and H. Hettema, POLCOR *package*, Nijmegen, 1992.
[41] H. Köppel, W. Domcke, and L. S. Cederbaum, Adv. Chem. Phys. **57**, 59 (1984).
[42] MOLPRO is a package of *ab initio* programs written by H.-J. Werner and P. J. Knowles, with contributions from R. D. Amos, A. Berning, D. L. Cooper *et al.*
[43] M. Abramowitz and I. A. Stegun, *Handbook of Mathematical Functions* (National Bureau of Standards, Washington, DC, 1964).
[44] G. Meijer (private communication).

Downloaded 11 Feb 2013 to 131.174.248.95. Redistribution subject to AIP license or copyright; see http://jcp.aip.org/about/rights_and_permissions